

DTIC FILE COPY

(2)

# Naval Ocean Research and Development Activity

May 1989

Report 182



## The Regional Polar Ice Prediction System— Barents Sea (RPIPS-B): A Technical Description

AD-A213 159

DTIC  
ELECTE  
OCT 04 1989  
S D 3 D

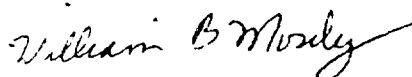
**Ruth H. Preller**  
**Shelley Riedlinger**  
Ocean Sensing and Prediction Division  
Ocean Science Directorate

**Pamela G. Posey**  
Berkeley Research Associates  
Springfield, Virginia

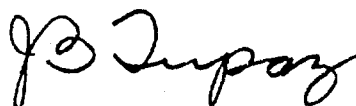
## Foreword

---

A knowledge of ice thickness, ice motion, and ice concentration (ice edge) is essential for effective, safe ship operations in polar regions. The time evolution of these parameters can impact the performance of weapons systems, acoustic surveillance capabilities, search and rescue planning, and other aspects of naval operations. The Naval Ocean Research and Development Activity has developed the first high-resolution sea-ice forecasting model for the Barents Sea based on the Hibler ice model. The model will run operationally at the Fleet Numerical Oceanography Center using ice thickness fields from the Polar Ice Prediction System as boundary conditions. Testing has shown that the high-resolution models are capable of better forecasting of the ice edge location and the growth (decay) and movement of ice near land boundaries. The operational version of the Barents Sea model will produce the same 14 sea-ice products for the Barents Sea, on a daily basis, that are presently produced by the Polar Ice Prediction System for the Arctic.



**W. B. Moseley**  
Technical Director



**J. B. Tupaz, Capt. in, USN**  
Commanding Officer

## Executive Summary

The hydrodynamic/thermodynamic Arctic sea-ice model designed by W. D. Hibler of the Cold Regions Research and Engineering Laboratory (CRREL) has been adapted to the Barents Sea. This model is driven by atmospheric forcing from the Naval Operational Global Atmospheric Prediction System (NOGAPS) and oceanic forcing from the Hibler and Bryan coupled ice-ocean model. This high-resolution model (25 km), which covers the entire Barents Sea and the western half of the Kara Sea, uses a 6-hour time step. Development of this model required the design of new ice inflow/outflow boundary conditions, which use the ice thickness fields from the Polar Ice Prediction System (PIPS) when inflow is indicated. Model results show good agreement with such data as the Naval Polar Oceanography Center's (NPOC) analysis of ice concentration and concentrations derived from passive microwave data. The model has a tendency, however, to melt ice too quickly in summer and to grow it back too slowly in the fall. Planned improvements in the atmospheric and oceanic forcing should correct this problem. The high resolution of the Barents Sea model enables it to predict the ice edge, ice growth and decay, and the movement of ice near land boundaries with greater accuracy than does the PIPS model. The Regional Polar Ice Prediction System for the Barents Sea (RPIPS-B) is the forecast system designed to run at the Fleet Numerical Oceanography Center (FNOC) based on the Barents Sea ice model. RPIPS-B is updated weekly by the NPOC analysis of ice concentration. The forecast system, presently in its "operational checkout" phase, is being made ready for a winter-spring operational test.

Accession For	
NTIS GRA&I	<input checked="" type="checkbox"/>
DTIC TAB	<input type="checkbox"/>
Unannounced	<input type="checkbox"/>
Justification	
By	
Distribution	
Availability Codes	
Date	Accession or Control
A-1	

## Acknowledgments

---

The authors would like to acknowledge the expert assistance of Mr. Ken Pollak and Mr. Tom Pham in the design and implementation of the Regional Polar Ice Prediction System for the Barents Sea.

This project was funded by the Office of Naval Research's Arctic Program (PE 61153N) under Dr. Thomas B. Curtin, and by the Space and Naval Warfare Systems Command through the Air Ocean Prediction Program (Program Element 63207N) under Captain J. J. Jensen.

# Contents

---

<b>I. Introduction</b>	<b>1</b>
<b>II. Model Description</b>	<b>1</b>
<b>III. The Model Grid</b>	<b>3</b>
<b>IV. Forcing</b>	<b>3</b>
<b>V. Initial Conditions</b>	<b>4</b>
<b>VI. Model Parameters</b>	<b>4</b>
<b>VII. Model Development</b>	<b>4</b>
<b>VIII. Example Output from RPIPS-B</b>	<b>7</b>
<b>IX. Summary and Conclusions</b>	<b>9</b>
<b>X. References</b>	<b>9</b>

# The Regional Polar Ice Prediction System—Barents Sea (RPIPS-B): A Technical Description

---

## I. Introduction

The capability to forecast sea-ice characteristics in the world's polar oceans has become a more viable task in recent years. The existence of increasingly more powerful computers, larger quantities of remotely sensed data, and the development of improved sea-ice models has contributed to the design of accurate sea-ice forecasting systems.

In September 1987, the Navy's Polar Ice Prediction System (PIPS) became an operational model at the Fleet Numerical Oceanography Center (FNOC). The model covers the central Arctic, the Barents Sea, and northern half of the Greenland and Norwegian Seas. PIPS is based on the Hibler ice model (Hibler, 1979; 1980). The ice model is driven by ocean currents and ocean heat fluxes derived from the Hibler and Bryan ice-ocean model (Hibler and Bryan, 1984; 1987). Atmospheric forcing for the model comes from the Navy's operational atmospheric forecast model, the Naval Operational Global Atmospheric Prediction System (NOGAPS) (Rosmond, 1981). PIPS makes a 120-hour forecast each day of such sea-ice characteristics as ice drift, ice thickness, and ice concentration (ice edge). The length of this forecast is based on the length of the NOGAPS forecast. The model is updated once a week by a digitized analysis field of ice concentration derived by the Naval Polar Oceanography Center (NPOC). On days when the update is not available, the model is restarted from its own 24-hour forecast fields (see Preller, 1985; Preller and Posey, 1989).

PIPS was originally designed to cover a large portion of the northern, ice-covered polar oceans. The resolution of PIPS was chosen to minimize the amount of computing time used in an operational forecast. Once PIPS became operational, higher resolution models designed to cover only one particular region of the Arctic would be developed and run operationally. The advantages of these high-resolution regional models are a more accurate prediction of the ice-edge location; greater accuracy in defining land boundaries, including island boundaries; and better resolution of straits.

The first such regional model, designed by the Naval Ocean Research and Development Activity (NORDA),

is a model for the Barents Sea. The Barents Sea model is similar to PIPS in design. The model uses the Hibler ice model as its basis and is driven by NOGAPS atmospheric forcing and the Hibler and Bryan ice-ocean model's oceanic forcing. The main difference between the two models is in the boundary conditions. PIPS uses solid-wall, closed boundaries everywhere except at the southern boundary between Greenland and Iceland and Iceland and Norway. This boundary can be simply treated as an ice outflow boundary. The Barents Sea model, however, required the development of new "ice" inflow/outflow boundary conditions.

This report provides a technical description of the Barents Sea model and presents results from both its development and operational checkout phases. The operational system for the Barents Sea will be referred to as the "regional PIPS for the Barents Sea," or RPIPS-B.

## II. Model Description

The regional Barents Sea model uses the Hibler dynamic/thermodynamic sea-ice model as its basis. The ice model is defined by five major components: momentum balance, ice rheology, ice thickness distribution, ice strength, and air/ice/ocean heat balance.

Although this model description is found in Preller and Posey (1989), it will be included in this report for the sake of completeness.

The momentum balance used to determine ice drift is given by

$$m \frac{D\vec{u}}{Dt} = m f \hat{k} \times \vec{u} + \vec{\tau}_a + \vec{\tau}_w - mg \text{grad } H + \vec{F},$$

where  $m$  is the ice mass per unit area,  $\vec{u}$  is the ice velocity,  $f$  is the Coriolis parameter,  $\vec{\tau}_a$  and  $\vec{\tau}_w$  are the air and water stresses,  $g$  is the acceleration of gravity,  $H$  is the sea surface dynamic height and  $\vec{F}$  is the force due to variation in the internal ice stress. Ice is considered to move in a two-dimensional field with forcing applied through simple planetary boundary-layer formulations.

The air and water stresses are defined using constant turning angles

$$\tau_a = \rho_a C_a |\vec{U}_g| (\vec{U}_g \cos \phi + \hat{k} \times \vec{U}_g \sin \phi)$$

$$\tau_w = \rho_w C_w |\vec{U}_w - \vec{u}| [(\vec{U}_w - \vec{u}) \cos \theta + \hat{k} \times (\vec{U}_w - \vec{u}) \sin \theta],$$

where  $\vec{u}$  is the ice drift velocity,  $\vec{U}_g$  is the geostrophic wind,  $\vec{U}_w$  is the geostrophic ocean current,  $C_a$  and  $C_w$  are the air and water drag coefficients,  $\rho_a$  and  $\rho_w$  are the air and water densities and  $\phi$  and  $\theta$  are the air and water turning angles. For a more detailed discussion of model dynamics and the spatial finite differencing code, see Hibler (1979).

The ice rheology, a viscous-plastic constitutive law, relates the ice stress to ice deformation and ice strength in the following manner:

$$\sigma_{ij} = 2\eta(\epsilon_{ij}, P) \epsilon_{ij} + [\xi(\epsilon_{ij}, P) - \eta(\epsilon_{ij}, P)]$$

$$\epsilon_{kk} \delta_{ij} - P\delta_{ij}/2,$$

where  $\sigma_{ij}$  is the two-dimensional stress tensor,  $\epsilon_{ij}$  is the strain tensor,  $P/2$  is a pressure term, and  $\xi$  and  $\eta$  are nonlinear bulk and shear viscosities. Ice flows plastically for normal strain rates and deforms in a linear viscous manner for small strain rates.

The ice thickness distribution takes into account the ice thickness evolution as a result of dynamic and thermodynamic effects. The regional Barents Sea model originally used a two-level approach (Hibler, 1979). This approach breaks ice into two categories, thick and thin, with the division between the two being 0.5 m. The compactness,  $A$ , is defined as the area within a grid cell covered by thick ice, while  $(1 - A)$  is the area covered by thin ice. This treatment resulted in an average ice thickness over the Arctic that was too thin when compared to observations (Preller et al., 1986). To correct for this bias and to include the strong dependence of ice growth rates on thickness, a seven-level ice thickness calculation used by Walsh et al. (1985) was added to the PIPS model in March 1988. This method divides the "thick" ice into seven categories and allows ice to grow/decay in each category. The seven levels are equally spaced between 0 and twice heff, where heff is the effective ice thickness (Hibler, 1979) or mean ice thickness over the entire grid cell. For periods of ice growth, snow cover is also divided into a seven-level linear distribution of snow depths equally spaced between 0 and 2 times the grid cell mean. When melting occurs, snow is assumed to be uniformly distributed over the ice covered portion of the grid cell. Snowfall rates are based on monthly mean climatological values (Maykut and Untersteiner, 1969; Parkinson and Washington, 1979). When tested on the PIPS model, this improved treatment of thick ice resulted in an average increase of ice thickness of 50 cm over the PIPS domain.

The equations for thickness and compactness are

$$\frac{\partial n}{\partial t} = - \frac{\partial(uh)}{\partial x} - \frac{\partial(vh)}{\partial y} + S_h + \text{diffusion}$$

$$\frac{\partial A}{\partial t} = - \frac{\partial(uA)}{\partial x} - \frac{\partial(vA)}{\partial y} + S_A + \text{diffusion},$$

where  $S_h$  and  $S_A$  are thermodynamic terms defined by

$$S_h = f\left(\frac{h}{A}\right) A + (1 - A) f(0)$$

$$S_A = \begin{cases} \frac{f(0)}{h_o} (1 - A) & \text{if } f(0) > 0 \\ 0 & \text{if } f(0) < 0 \end{cases}$$

$$+ \begin{cases} 0 & \text{if } S_h > 0 \\ \left(\frac{A}{2h}\right) S_h & \text{if } S_h < 0 \end{cases},$$

with  $f(h)$  as the growth rate of ice of thickness  $h$  (heff) and  $h_o$  a fixed demarcation between thick and thin ice. In all model simulations,  $h_o = 0.5$  m. In the seven-level ice thickness calculation, heff is the seven-level sum of ice thickness, including the calculated snow and ice thickness changes. The term  $S_h$  is the net growth or melt of ice.  $S_A$  is the change in compactness due to the growth or decay of ice.

Ice strength is treated as a function of the ice thickness distribution and compactness given by the equation

$$P = P^* h \exp[-C(1 - A)],$$

where  $P^*$  and  $C$  are fixed empirical constants,  $h$  is the ice thickness, and  $A$  is the compactness. This relationship shows the strength of ice to be strongly dependent on the amount of thin ice  $[(1 - A)]$ . It also allows the ice to strengthen as it becomes thicker.

The thermodynamic portion of the code determines growth and decay rates of ice based on a heat budget balance between the atmosphere, the ice, and the ocean, including the effects of heat absorbed by leads via lateral mixing. Similar to Semtner's (1976) formulation, heat is transferred through the ice by assuming a linear temperature profile along with a constant ice conductivity. When open water is losing heat to the atmosphere, the heat budget growth rates are taken to be vertical growth rates. When open water absorbs heat, the heat mixes underneath the flows to reduce the vertical growth rate. Any remaining heat can either cause lateral melting or raise the temperature of the mixed layer. In the presence of an ice cover,

the mixed-layer temperature is always set equal to freezing. Thus, excess heat absorbed by leads is used for lateral melting until the ice disappears. During growth conditions, ice cannot form until the mixed layer reaches the freezing temperature of seawater.

In the two-level version of the model (following Bryan et al., 1975 and Manabe et al., 1979), the effects of snow cover are treated such that the ice surface albedo is that of snow (0.75) when the calculated surface temperature is below freezing and that of snow-free ice (0.66) when the surface temperature is at the melting point. Thus, the upward heat flow,  $I_h$ , through ice of thickness  $h$  is

$$I_h = (K/h) (T_w - T_o),$$

where  $K$  is the ice conductivity,  $T_w$  is the water temperature, and  $T_o$  is the surface temperature of the ice.

In the two-level case, snow is parameterized only through the surface albedos, but the new seven-level formulism uses the accumulated rates from Maykut and Untersteiner (1969) and Parkinson and Washington (1979). The thermal conductivity in the seven-level case is a single value based on a weighted sum of snow and ice conductivities

$$\frac{K_s K_i}{(K_s S n_{LVL} + K_i h_{LVL})},$$

where  $h_{LVL}$  is the ice thickness at that level,  $S n_{LVL}$  is the snow depth at the same level,  $K_s$  is the snow conductivity, and  $K_i$  is the ice conductivity. The prescribed surface albedos used by Walsh et al. are 0.80 for snow and 0.65 for ice.

The surface heat budget, after Parkinson and Washington (1979) and Manabe et al. (1979), is given by

$$\begin{aligned} (1 - \alpha) F_s + F_l + D_l |\vec{U}_g| (T_a - T_o) \\ + D_2 |\vec{U}_g| [q_a(T_a) - q_s(T_o)] \\ - D_3 T_o^4 + (K/H) (T_w - T_o) = 0, \end{aligned}$$

where  $\alpha$  is the surface albedo,  $T_o$  is the surface temperature of ice,  $T_a$  is the air temperature,  $T_w$  is the water temperature,  $\vec{U}_g$  is the geostrophic wind,  $q_s$  is the specific humidity of the ice surface,  $F_s$  is the incoming short-wave radiation,  $F_l$  is the incoming long-wave radiation,  $D_l$  is the bulk sensible heat transfer coefficient,  $D_2$  is the bulk latent heat transfer coefficient (water or ice), and  $D_3$  is the Stephan-Boltzman constant times the surface emissivity. This surface heat budget defines a surface temperature for the ice that balances the heat budget. This temperature then determines the conduction of heat through the ice and the growth rate. If the derived temperature is above freezing, it is set back to the freezing point.

Surface and bottom ablation rates are then determined by the imbalances in the surface heat budget and by conduction of heat into the mixed layer. Heat transfer from the deep, warmer, ocean water can either be treated as a constant or as a variable heat flux into the mixed layer. For a detailed discussion of the thermodynamic portion of the model, see Hibler (1980).

### III. Model Grid

The Barents Sea model grid was designed as a subsection of the FNOC northern hemisphere polar stereographic grid. The model grid covers the entire Barents Sea and the western half of the Kara Sea. An averaged mapping factor is used to approximate equal spacing for the FNOC polar stereographic grid in the Barents Sea domain. The ice model grid is defined as an equally spaced, 25-km grid, subset of the FNOC northern hemisphere polar stereographic grid. The resultant ice model dimensions are 74 × 66 (Fig. 1).

Boundaries of the model are solid walls except for the boundary between Spitzbergen and Norway. This region contains two rows of "outflow" grid cells. Ice can only be transferred into these grid cells by advection and once there, flows out of the basin. The boundaries between Spitzbergen and Franz Josef Land, Franz Josef Land and Novaya Zemlya, and Novaya Zemlya and the Soviet coast are all inflow/outflow boundaries. Details of the model's inflow/outflow boundary conditions will be described in the model development section VII B.

### IV. Forcing

The Barents Sea model is driven by both atmospheric and oceanic forcing. The atmospheric forcing is obtained from the NOGAPS model. This global atmospheric model provides surface pressure fields (NOGAPS field A01), which are used to determine geostrophic winds. In addition to surface pressure, the NOGAPS model also provides surface vapor pressure (A12), which is used in conjunction with surface pressure to determine the specific humidity at the ice surface; surface air temperature (A07); incoming solar radiation (short wave-A11); sensible heat flux (A16); and total heat flux (A18). These last three fields are used to determine long-wave radiation.

Monthly mean geostrophic ocean currents and deep-ocean heat fluxes derived from the Hibler/Bryan coupled ice-ocean model are used as the ocean forcing for the model. The effects of the variability of ocean currents on ice drift has been shown to be of importance over long time scales (Thorndike and Colony, 1982). On the time scale of a forecast (5 days), the variability of the ocean currents has a much smaller effect on the ice drift than the variability of the wind stress fields.



For this reason, monthly mean ocean currents can be used as a reasonable estimate for oceanic forcing.

Including monthly mean, deep-ocean heat fluxes has resulted in a tremendous improvement in the model's capability to predict edge location in the marginal ice zone. Hibler and Bryan (1984; 1987) have shown that this oceanic heat flux can melt large amounts of ice in the marginal ice zone. A drastic improvement in ice-edge location was seen in the results of the PIPS model when monthly mean, deep-ocean heat fluxes were included (Preller, 1985; Preller and Posey, 1989). The Barents Sea model required some adjustment to the original Hibler and Bryan heat fluxes. This correction to the heat fluxes is discussed in section VII A.

Both PIPS and RPIPS-B forecasts could be improved by improving the atmospheric and oceanic forcing. Oceanic forcing would be improved by having an ocean model coupled to the ice model. This model could predict the variability of the ocean on the same time and space scales as the ice. Higher resolution in the atmospheric models would also improve the forecast capability. At present, NOGAPS resolution is approximately 400 km, but RPIPS-B is 25 km. The development of such models is a task being researched in both the (6.1 and 6.2) communities.

## V. Initial Conditions

During the development of the Barents Sea model, the model was spun up to a cyclic "equilibrium state," where ice thickness, ice velocity, and ice concentration take on similar values on corresponding days of successive years. Initialization for the equilibrium state case requires setting ice drift velocities to zero and ice thickness to a constant value of 1.1 m ( $1.0 \times 10^3 \text{ kg m}^2 / \rho_i$ ) and ice concentration to 100% at all grid points. From these initial conditions, it takes approximately 2 years of model integration to reach a cyclic equilibrium state. One particular year of NOGAPS forcing is used repeatedly to reach the equilibrium state.

RPIPS-B can be initialized in three different ways. Each day the model is run making a 120-hour forecast. The model's 24-hour forecast of ice thickness, concentration, ice drift, surface ice temperature, and heat absorbed by the open ocean is saved each day. The model uses this 24-hour forecast as its restart field the next day. If the restart field from the previous day is not available, then the model searches back as far as 1 week. If no restart fields can be found, then model climatology is used to restart the model. The model climatology contains monthly mean fields derived from the Barents Sea "cyclic steady state" results driven by 1986 NOGAPS forcing.

Once per week (usually Friday), in addition to the restart field, the model is also given a new field of

gridded ice concentration. This concentration field is a digitized version of the NPOC weekly ice concentration analysis. The NPOC analysis is a subjective analysis derived from available remotely sensed data (Advanced Very High Resolution Radiometer, Visible, Passive Microwave) and available observations (ship, plane, etc.) (Naval Polar Oceanography Center, 1986). This field is hand-digitized once per week by NPOC and transferred to FNOC. The digitized data are then placed on the model grid and used to update the model.

The data are assimilated into the Barents Sea model in the following manner. The model's restart field is found (either a 24-hour forecast or climatology). RPIPS-B then checks to see if an NPOC analysis field is available. If the analysis field is older than 4 days or has been used within the past 4 days, then an update is not made. Otherwise, if the NPOC analysis is available, then the model's forecasted ice concentration field is entirely replaced by the NPOC analysis. Two additional fields are then updated: the ice thickness and the heat stored by the ocean. The new concentration field is compared to the model-derived concentration field. If no ice exists where it existed before the update, then the ice thickness is set equal to zero and a small amount of heat is added to the open-ocean mixed layer. If concentration has been added to a previous open ocean region, then ice thickness is updated in the following manner:

If  $0.15 < A < 0.5$  and  $H < 0.2$ , then  $H = 0.2$

or

If  $A > 0.5$  and  $H < 0.2$ , then  $H = 0.4$ .

and heat is removed from the mixed layer.

## VI. Model Parameters

The Barents Sea model uses a 6-hour timestep. In the initial model testing, atmospheric forcing fields were interpolated from the  $63 \times 63$  northern hemisphere polar stereographic grid used by FNOC to the Barents Sea grid. Ocean forcing is updated once per month. Turning angles for the geostrophic wind and drag coefficients were based on values derived from the testing of PIPS (Preller and Posey, 1989). Additional parameters used by the model are given in Table I.

## VII. Model Development

The Barents and Kara Seas are both Arctic marginal seas. The Barents Sea is bounded by Spitzbergen and Franz Josef Land to the north, and to the west by a line running north from North Cape through Bear Island to the southern tip of Spitzbergen. The Barents and Kara Seas are separated by the island of Novaya Zemlya, which restricts the transport of ice between

them. These seas are both relatively shallow; the Barents Sea, the deeper of the two, averages 200 m in depth.

The Kara Sea is typical for its high northern latitude. It has a solid ice cover during the winter and is ice-free during the summer, except for the extreme northern part. As the warmest of the Arctic seas, the Barents Sea is atypical. It is strongly influenced by the warm, saline Atlantic waters of the Norwegian Current. As a result, the southwestern third of the Barents Sea remains ice-free throughout the year.

The composition of the sea ice in the Barents Sea is usually complex and is composed of many different ice types. The majority of the ice is first-year ice formed locally, but some multiyear ice is transported from the Arctic Ocean between Spitzbergen, Franz Josef Land, and the northern tip of Novaya Zemlya. Multiyear ice can also form locally around some of the islands, and icebergs frequently occur in the Barents Sea. During the summer, the ice retreats far to the north and the Barents Sea becomes ice-free. In winter, the ice edge advances until it extends over the Spitzbergen Bank to Bear Island. The ice often extends well off the coast of Novaya Zemlya and over the shelf off the Soviet coast (the Pechora Sea) and into the White Sea.

Year-to-year variability of the ice extent in the Barents Sea is strong. Parkinson et al. (1987) studied Arctic sea ice using passive microwave data from the Nimbus-5 Electrically Scanning Microwave Radiometer (ESMR) from 1973 to 1976. They found that the timing of the maximum extent of ice varies from year to year

and is most likely due to a combination of atmospheric and oceanic effects. Figure 2 shows their calculation of the yearly cycle of sea-ice cover from 1973 to 1976. Note that a maximum occurs in February 1973 and that a double maximum occurs during February and April 1974. The maximum is in March and April 1975, while maxima occur in January and March 1976. Summer-time variability is also apparent from the change in the amount of ice area existing in August and September from year to year.

Year-to-year variability is also seen in the climatological minimum and maximum extension of sea ice in the Barents Sea from the Navy-NOAA Joint Ice Center (Fig. 3). Despite these yearly variations, the seasonal pattern of growth and decay in the Barents Sea is similar from year to year, with the maximum extension of the ice usually falling in the February-April time frame and the minimum occurring in August-September (Parkinson et al., 1987; Loeng, 1979; Loeng and Vinje, 1979).

### A. Ocean Currents and Heat Fluxes

The location of the ice edge is strongly influenced by the heat brought into the Barents Sea from the southwest via the Norwegian Atlantic Current. The Norwegian Coastal Current flows along the coast of Norway. Paralleling this coastal current is the Norwegian Atlantic Current. Off the coast of northern Norway, this current splits in two: one branch flows northward and becomes the West Spitzbergen current; the other branch enters the Barents Sea as the

Table 1. Parameters used in RPIPS-B.

Parameter	Definition	Value
$C_a$	Drag coefficient of air	0.0008
$C_w$	Drag coefficient of water	0.0055
$C$	Empirical constant in the strength equation	20
$e$	Ratio of the principal axis of the elliptic yield equation	2
$f$	Coriolis parameter	$1.46 \times 10^{-4} \text{ sec}^{-1}$
$h_o$	Thickness limit between thick and thin ice	0.5 m
$\rho_i$	Density of ice	$0.91 \times 10^3 \text{ kg m}^{-3}$
$\rho_a$	Density of air	$1.3 \text{ kg m}^{-3}$
$P^*$	Pressure constant	$2.75 \times 10^4 \text{ N m}^{-2}$
$\Delta x = \Delta y$	Horizontal grid spacing	25 km
$\Delta t$	Time step	6 hour
$\zeta_{\max}$	Nonlinear bulk viscosity	$(P/4) \times 10^9 \text{ kg s}^{-1}$
$\eta_{\max}$	Nonlinear shear viscosity	$\zeta_{\max}/e^2$
$\phi$	Turning angle of air	$23^\circ$
$\theta$	Turning angle of water	$25^\circ$
$H_i$	Initialization ice thickness	1.1 m

North Cape Current. Figure 4 is a simplified depiction of the surface current system from Midthun and Loeng (1987), based on current maps by Lantsuura (1959) and Novitskiy (1961). The southern part of the North Cape Current continues eastward with the Norwegian Coastal Current and becomes the Murman Current. The northern part of the North Cape Current splits into three branches. One branch proceeds northward between Hopen Island and the Great Bank until it submerges under Atlantic water. The second branch continues eastward between the Great Bank and the Central Bank as an intermediate current. The third branch turns southeastward and parallels the Murman current off the coast of the Soviet Union and then turns northeastward along the axis of the eastern basin off the coast of Novaya Zemlya. The colder, less saline Arctic water enters the sea as two currents, one along the east coast of Spitzbergen and one between Franz Josef Land and Novaya Zemlya (Dickson et al., 1970). The first current, the East Spitzbergen current, continues southward along the coast of Spitzbergen. The second current, the Persey Current, flows southwestward, south of Franz Josef Land, along the eastern slope of the Svalbard Bank and around Bear Island.

Examples of the ocean currents used in the Barents Sea model are shown in Figures 5a and 5b. As stated, these monthly mean values are derived from the Hibler and Bryan ice-ocean model. These currents follow the general pattern described above. However, due to the coarse resolution of the Hibler and Bryan model ( $\approx 160$  km), some of the detail of the current pattern is lost. In most of the monthly mean currents, the inflowing Atlantic water breaks up into two as opposed to three branches; one moves to the east along the Norwegian coast, and a second enters the Barents Sea and turns toward the northeast. During most months, the current enters the Barents Sea between Franz Josef Land and Novaya Zemlya, flows toward the southwest, and curves back toward the north. Part of this current exits through the region between Franz Josef Land and Spitzbergen, and part flows along Spitzbergen and out of the Barents Sea near Bear Island (Fig. 5a). During October and November, however, the flow exits the Barents Sea through the passage between Franz Josef Land and Novaya Zemlya (Fig. 5b).

The heat fluxes associated with these currents for the Hibler and Bryan modeled region are shown in Figure 6. This result indicates that large heat fluxes are carried into the south-western third of the Barents Sea. The monthly mean heat fluxes in the Barents Sea grid are shown in Figures 7a and 7b. Figure 7a is the original monthly mean heat flux field from the ice-ocean model. After extensive testing of the model with these heat fluxes, it was determined that the fluxes were too weak in the south-central portion of the Barents Sea. As a result, this region always contained too much ice. These weak heat fluxes appear

to be a result of the resolution of the Hibler and Bryan ice-ocean model. Using 160 km grid spacing, the model cannot accurately resolve some features of the ocean current field. As a result, the current field is smoothed and can be weaker than observed. Weak currents would not penetrate far enough east into the Barents Sea to bring the heat from the Norwegian current necessary to keep the region ice-free. To correct for this excessive amount of ice, the heat fluxes were expanded to cover a larger part of the eastern Barents Sea. These heat fluxes were adjusted so that the new ice edge location agreed closely with the NPOC (1986) ice edge. New heat fluxes were created by averaging adjacent row (column) values and inserting the new average values between the old rows (columns). This was done in such a way that the large heat flux values were expanded and the low values close to land boundaries were eliminated. Figures 8a and 8b show the improvement to the ice edge location when the model was driven by 1983 NOGAPS forcing and the adjusted heat fluxes. Figures 9a and 9b show the improvement in model results when the model was driven by 1986 NOGAPS forcing and the adjusted heat fluxes. The correction to the heat fluxes was chosen as the best average adjustment between results using the two years of atmospheric forcing.

## B. Open Boundary Conditions

In the initial testing of the Barents Sea model, it became obvious that the region required ice inflow/outflow boundary conditions. Prior to this, both PIPS and tests performed by Hibler had used only ice outflow boundary conditions.

The first test of the model boundaries treated all boundaries as solid walls except for the boundary between Spitzbergen and Norway. That boundary is treated as an ice outflow boundary in all of the test cases. Ice can be transferred into these grid cells only by advection and, once there, is removed from the basin. Allowing outflow only at this boundary is a valid assumption, since most of the flow is into the Barents Sea on the southern, ice-free half of the boundary and out of the Barents Sea on the northern side of the boundary where ice can exist. It should also be noted that these early tests were performed on a version of the model that excluded the Kara Sea. When the northern boundaries of the model were kept closed, the model gave very unrealistic results. If the wind forcing blew across these boundaries from the north, then ice was pushed away and huge leads or regions of open water appeared at the solid wall boundary. If the wind forcing was from the south, then ice would "pile up" unrealistically at the boundary (Fig. 10a).

In the second case, the boundary between Franz Josef Land and Novaya Zemlya was designated an ice "inflow/outflow" boundary. The interior outflow boundary is the first interior "common" grid cells

between Franz Josef Land and Novaya Zemlya. For each time step, the model checks the ice drift at each grid cell on the boundary. If drift implies that ice is flowing out of the basin, then the standard Hibler ice outflow boundary condition is used. If the drift indicates inflow, a specified amount of ice thickness is placed into the grid cell and is allowed to advect into the model. The amount of ice placed into the grid cell is determined in one of two ways. In the early testing of the model, the value of inflowing ice was set to a constant 0.5 m for all months of the year, except August and September, when it is set equal to 0.0 m. During these 2 months, the region north of the Barents Sea is most often ice-free. This value proved to be a good average for ice inflowing at that boundary. In RPIPS-B and additional model test cases, the ice thickness derived from the PIPS model is interpolated to the Barents Sea model grid and used as the ice inflow value. Although the second method is more accurate, the constant value used in the first method was very useful in that it allowed the Barents Sea model to be run as a "stand-alone" model. That is, it allowed many test cases to be run when the PIPS-interpolated ice thickness values were not available. Figure 10b shows a result identical to that of Figure 10a, except that the boundary between Franz Josef Land and Novaya Zemlya has been opened and a 0.5-m average ice thickness applied at the inflow/outflow boundary. This result was in much better agreement with the NPOC analysis than the closed boundary result.

In the third test case, the same inflow/outflow boundary condition was added to the boundary between Franz Josef Land and Spitzbergen. Figure 11a shows the result when this boundary was closed and Figure 11b is the identical case result with the boundary open to inflow and outflow. Again, opening this boundary resulted in a much more realistic solution.

In the RPIPS-B model and the remaining test cases, the western Kara Sea was added to the model. In the Kara Sea, however, the constant value of 0.5 m is used as the boundary condition. This method was chosen because the PIPS grid does not cover all of the Kara Sea.

The remaining test cases discussed in this report and the RPIPS-B model use open inflow/outflow boundary conditions from PIPS at the boundaries between Spitzbergen and Franz Josef Land and between Franz Josef Land and Novaya Zemlya, and a constant value inflow/outflow boundary condition between Novaya Zemlya and the Soviet coast (Kara Sea). The western boundary between Spitzbergen and Norway is treated as an ice outflow boundary condition in all cases.

## VIII. Example Output from RPIPS-B

Results from the Barents Sea model test cases using 1983 and 1986 NOGAPS atmospheric forcing, along

with results from the RPIPS-B operational check-out (OPCHECK), will be presented in this section. During OPCHECK, the model jobstream is run to show that the job can perform in an operational environment without disruption of the operational run. It also provides an opportunity for minor improvements to be made to the model. The main difference between the Barents Sea model test results and the RPIPS-B results is that RPIPS-B results are updated weekly by the NPOC analysis of ice concentration. Model results will be examined in terms of ice drift, ice thickness and ice concentration (ice edge).

A number of similar tendencies appear in Barents Sea model solutions using both the 1983 and 1986 NOGAPS forcing. Therefore, we will present results from the evolution of the 1983 test case to imply that a similar situation existed in the 1986 case. The Barents Sea model was shown to take, at most, two years to spin up to a cyclic equilibrium solution. Figures 12a and 12b show the March mean thickness field for the first and second year of spin-up. The model 1983 test run was initialized on January 18 using forcing from NOGAPS and the initial conditions described in section V. The model is integrated out for 3 years using 1983 NOGAPS forcing to drive the model each year. The main difference between the first-year and second-year results appear in the ice thickness fields near Spitzbergen and Franz Josef Land. These results imply that the model needs longer than 2 months of spin-up time (Fig. 12a) to build up thick ice along these islands (Fig. 12b). The third year monthly mean ice-thickness field is identical to the second-year ice thickness and is not shown.

Figure 13 shows the RPIPS-B grid with four transect lines overlaid at points  $J = 5, 20, 35$  and  $50$ . Figures 14a-d show March monthly mean ice thickness along each transect for the first and second year of model integration. The largest difference from year 1 to year 2 lies along the transect at  $J = 5$ , Figure 14a. This transect runs along the eastern side of Spitzbergen and shows the piling up of ice along this coast during the second year winter. Transects from the third year of integration are identical to the second-year transects and are not shown.

The Barents Sea is observed to have its most extensive ice cover in the winter months (February and April) and to become ice-free or nearly ice-free in the summer (August and September). Model results develop a similar seasonal pattern, with the Barents Sea becoming ice-free during the first summer of the spin-up testing. Results show that after the first year's summer melting of ice the model quickly reached a near-equilibrium state by fall of the first year. Figures 15a and 15b are November mean ice thicknesses from the first and second year of model integration. Only small differences, again, in the region between Spitzbergen and Franz Josef Land, can be seen.

Figures 16a-d show November mean thicknesses along the four transects indicated in Figure 13. Aside from the small increase in ice thickness at transect J = 5, these figures show little change in ice thickness from year 1 to year 2.

Equilibrium results from both the 1983 and 1986 test cases showed that the thickest ice in the Barents Sea occurs in the winter months on the eastern coast of Spitzbergen, where model thicknesses are approximately 4 m. Throughout the rest of the Barents Sea, the ice thickness averages about 1 m. During the summer months, when ice is present, it averages less than 1 m thick.

Ice drift in the Barents Sea is closely correlated to the winds. The ice drift from the Barents Sea model responds rapidly to the wind forcing. This rapid response to the winds has been observed in the Barents Sea (Vinje, 1985).

Ice-thickness values in many parts of the Barents Sea appear to be closely linked to the wind forcing. Figures 17a and 17b show April monthly mean ice drift and ice thickness from 1986. Monthly mean winds during this period were blowing toward the south and the southeast. As a result, ice piled up on the western side of Novaya Zemlya and along the Soviet coast in the Kara Sea. Figures 18a and 18b show that in May, the mean winds changed, causing the ice to drift away from the Soviet coast, away from the west coast of Novaya Zemlya, and into the east coast of Spitzbergen. Correspondingly, the ice thinned along the Soviet coast and the west coast of Novaya Zemlya and piled up along the east Spitzbergen coast.

The high resolution of the Barents Sea model allows for realistic simulations of ice moving toward or away from model coastlines that are not possible in the lower-resolution PIPS model. Regions of thin ice or open water, induced by wind forcing, are often observed in satellite imagery (Fig. 19) taken along the coastlines in the Kara Sea and along the coasts of Novaya Zemlya. The Barents Sea model is capable of reproducing similar wind-induced features in the ice thickness field.

Monthly mean ice concentrations, the percentage of a grid cell covered by thick ice, are shown in Figures 20a and 20b for 1983 and in Figures 21a and 21b for 1986. The NPOC analysis is overlaid on the winter and fall examples. The Barents Sea model tests show that the model results generally agree with observations at all times of year except during the summer. The Barents Sea model becomes ice-free too early in the summer (usually mid- to late July) and grows ice back too late in the fall (mid- to late October). The NPOC analysis shows the Barents Sea becoming ice-free from mid- to late August and shows ice growing back in early October. This indicates that the Barents Sea model becomes too warm in the summer. The extra heat that

keeps the Barents Sea model ice-free comes from a combination of heating by both the atmosphere and the ocean. This problem could be corrected with improved atmospheric forcing in the Arctic and improved ocean forcing via a coupled ice-ocean model. These improvements are presently being addressed by FNOC and NORDA, and the problem is being corrected RPIPS-B by updating the model with the NPOC analysis. This update places ice in the model, according to the NPOC analysis, and removes the excess heat.

Year-to-year variability in sea-ice extent, similar to that seen by Parkinson et al. (1987) is apparent in the model results. Figure 22 is a calculation of the yearly sea-ice cycle from the Barents Sea test cases using 1983 and 1986 NOGAPS forcing. In 1983, a double maximum in ice extent occurred in February and in April and May, similar to the Parkinson et al. results for 1974 (Fig. 2b). The 1986 Barents Sea model results showed a peak in March and a decrease in April and May, similar to the 1976 ESMR data (Fig. 2d). Model results also indicated a greater ice extent in 1986 than in 1983 ( $1.4 \times 10^6 \text{ km}^2$  vs.  $1.2 \times 10^6 \text{ km}^2$ ). NPOC analyses for these 2 years support this trend except in April 1986. The NPOC analysis showed ice cover as extensive in April as it was in March. These figures also demonstrate that the Barents Sea model melts too much ice in the summer of both years. Ice melted earlier in July 1983 than in July 1986, but also grew back more quickly in November 1983. This trend also appeared in the NPOC analysis.

RPIPS-B began to run in an OPCHECK mode in the fall of 1988. During the model OPCHECK, the following fields were used for testing:

1. Cumulative ice drift—Tau 24, Tau 120
2. Ice thickness—Tau 24, Tau 120
3. Ice concentration—Tau 24, Tau 120.

It is planned that the operational version of RPIPS-B will generate the same product fields as PIPS (Prieller and Posey, 1989).

As stated previously, the only difference between RPIPS-B and the Barents Sea test cases is that the model is updated weekly with ice concentration data from NPOC. Both PIPS and RPIPS-B are updated by the same NPOC analysis each week. The finer resolution of RPIPS-B, however, allows for a more detailed, accurate update of the ice edge in the Barents Sea. Figure 23 is the NPOC analysis for 28 December 1988. Figures 24a and 24b show the model solutions after an update from this NPOC analysis for both PIPS and RPIPS-B. Note that the higher resolution and larger areal extent of RPIPS-B is responsible for the detailed ice edge along Novaya Zemlya and the Soviet coast. The resolution of RPIPS-B also allows for better definition of the ice protrusion located near 73°N and 40°E.

## IX. Summary and Conclusions

RPIPS-B, the FNOC version of the Barents Sea model, is presently in its OPCHECK phase being prepared for a winter/spring OPTTEST. In its development stage, the Barents Sea model was spun up to a cyclic equilibrium state using atmospheric forcing from NOGAPS and oceanic forcing from the Hibler and Bryan ice-ocean model. New ice inflow/outflow boundary conditions were designed for the northern boundaries of the model.

Model test results compared well with observations (NPOC analysis). Results also showed that the finer resolution of RPIPS-B enabled far better predictions than PIPS of ice-edge location, ice thickness, and ice movement in the Barents Sea, particularly near land boundaries.

As a forecast tool, RPIPS-B will be run daily, making a 120-hour forecast. The model will be run after PIPS and will use the ice thickness field from PIPS at its inflow/outflow boundary. RPIPS-B will produce the same 14 product fields presently produced by PIPS.

## X. References

- Bryan, K., S. Manabe, and R. Pacanowski (1975). A Global Ocean-Atmosphere Climate Model, Part II—The Oceanic Circulation. *Journal of Physical Oceanography* 5:30-46.
- Dickson, R. R., L. Midttun, and A. Mukhin (1970). The Hydrographic Conditions in the Barents Sea in August-September 1965-1968. In *International O-group Fish Surveys in the Barents Sea 1965-1968*, O. Dragesund (ed.), Int. Coun. Explor. Sea, Cooperative Res. Rep., Ser. A, No. 18.
- Hibler, W. D. (1979). A Dynamic/Thermodynamic Sea Ice Model. *Journal of Physical Oceanography* 9:815-846.
- Hibler, W. D. (1980). Modeling a Variable Thickness Sea Ice Cover. *Monthly Weather Review* 108:1944-1973.
- Hibler, W. D. and K. Bryan (1984). Ocean Circulation: Its Effects on Seasonal Sea-Ice Simulations. *Science* 224:489-491.
- Hibler, W. D. and K. Bryan (1987). A Diagnostic Ice-Ocean Model. *Journal of Physical Oceanography* 17:987-1015.
- Loeng, H. (1979). A Review of the Sea Ice Conditions of the Barents Sea and the Area West of Spitzbergen. *Fisken Hav.* 2:29-75 (in Norwegian; abstract in English).
- Loeng, H. and T. Vinje (1979). On the Sea Ice Conditions in the Greenland and Barents Sea. *POAC 79, Proceedings of the Fifth International Conference of Port and Ocean Engineering and Arctic Conditions*, The Norwegian Institute of Technology, Trondheim, Norway.
- Manabe, S., K. Bryan, and M. Spelman (1979). A Global Ocean-Atmosphere Climate Model With Seasonal Variation for Future Studies of Climate Sensitivity. *Dynamics of Atmosphere and the Ocean* 3:393-426.
- Maykut, G. A. and N. Untersteiner (1969). *Numerical Prediction of the Thermodynamic Response of Arctic Ice to Environmental Changes*. The Rand Corporation, Santa Monica, California, RM-6093-PR.
- Midttun, L. and H. Loeng (1987). Climatic Variations in the Barents Sea. *Proceedings of the Third Soviet-Norwegian Symposium*, Murmansk Institute Marine Research, Bergen, Norway.
- Naval Polar Oceanography Center (1986). *Eastern-Western Arctic Sea Ice Analysis 1986*. Washington, D. C.
- Novitskiy, V. P. (1961). Permanent Currents of the Northern Barents Sea. *Trudy gos. okeanogr. Inst.* 64:1-32 (in Russian).
- Parkinson, C. L. and W. Washington (1979). A Large-Scale Numerical Model of Sea Ice. *Journal of Geophysical Research* 84:311-337.
- Parkinson, C. L., J. Comiso, J. Zwally, D. Cavalieri, P. Gloersen, and W. Campbell (1987). *Arctic Sea Ice 1973-1976: Satellite Passive-Microwave Observations*. National Aeronautics and Space Administration, Washington, D. C., NASA SP-489.
- Preller, R. H. (1985). *The NORDA/FNOC Polar Ice Prediction System (PIPS)—Arctic: A Technical Description*. Naval Ocean Research and Development Activity, Stennis Space Center, Mississippi, NORDA Report 108.
- Preller, R. H., P. G. Posey, K. D. Pollak and R. M. Clancy (1986). Forecasting Ice Thickness and Concentration in the Arctic Using a Numerical Model. *Proceedings of the Second Workshop on Ice Penetration Technology*, U.S. Army Cold Region Research and Engineering Laboratory, Hanover, New Hampshire.
- Preller, R. H. and P. G. Posey (1989). *The Polar Ice Prediction System—A Sea Ice Forecasting System*. Naval Ocean Research and Development Activity, Stennis Space Center, Mississippi, NORDA Report 212.
- Rosmond, T. E. (1981) NOGAPS: Navy Operational Global Atmospheric Prediction System. In *Fifth Conference on Numerical Weather Prediction* (Monterey, California), American Meteorological Society, Boston, Massachusetts, preprint volume, 74-79.
- Semtner, A. J., Jr. (1976). A Model for the Thermodynamic Growth of Sea Ice in Numerical Investigations of Climate. *Journal of Physical Oceanography* 6:379-389.
- Tantsiura, A. I. (1959). About the Current in the Barents Sea. *Trudy polyar. nauchno-issled. Inst.morsk.ryb.Khoz.Okeanogr.*, 11:35-53 (in Russian).
- Thorndike, A. S. and R. Colony (1982). Sea Ice Motion in Response to Geostrophic Winds. *Journal of Geophysical Research* 87:5845-5892.

Vinje, T. (1985). *Physical Environment Western Barents Sea: Drift, Composition, Morphology and Distribution of the Sea Ice Fields in the Barents Sea*. Norsk Polarinstitutt, Oslo, Skrifter No. 179c.

Walsh, J. E, W. Hibler, and B. Ross (1985). Numerical Simulation of Northern Hemisphere Sea Ice Variability, 1951-1980. *Journal of Geophysical Research* 90:4847-4865.

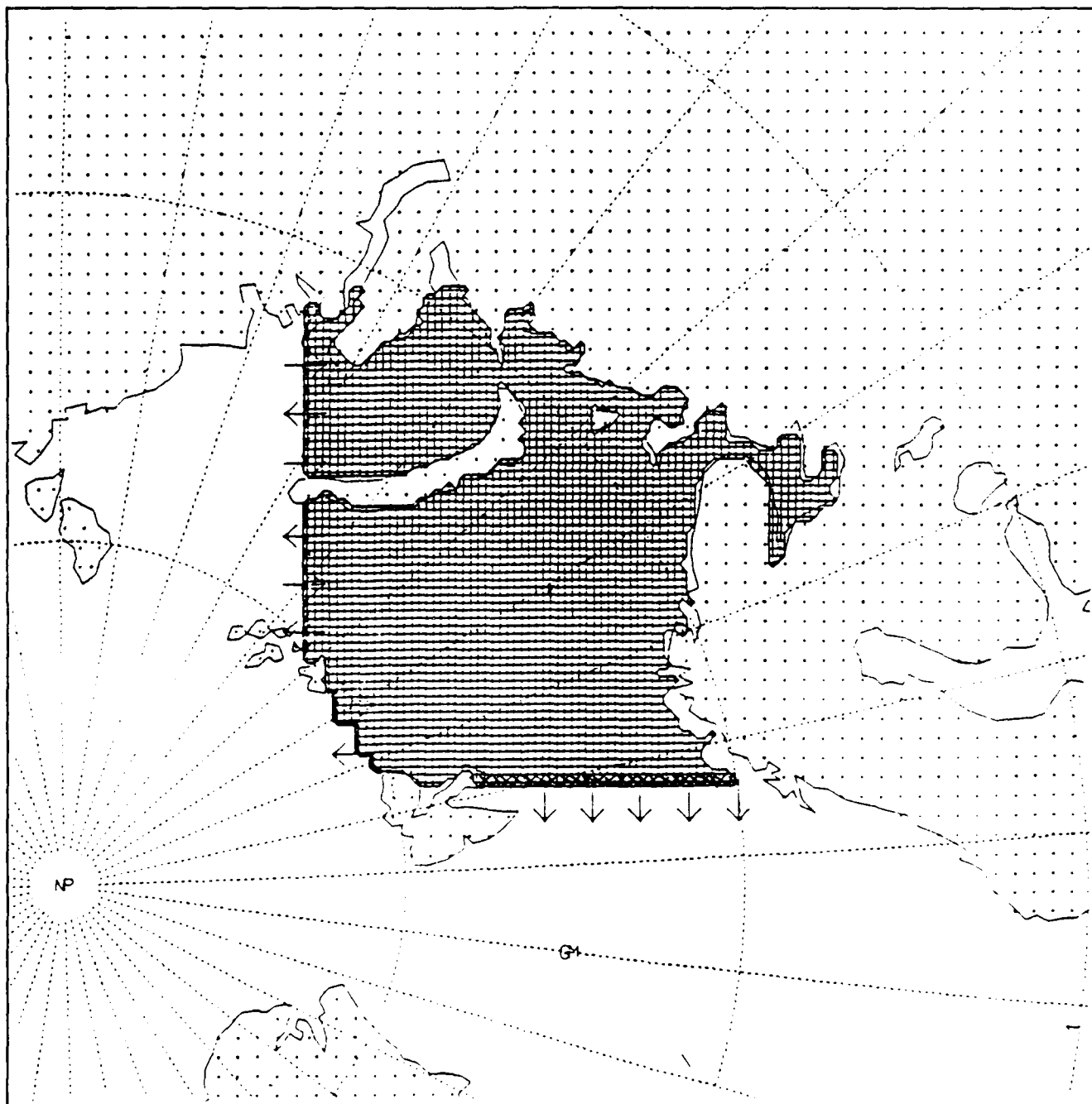


Figure 1. Barents Sea model grid with arrow indicating outflow and inflow/outflow boundaries. Inflow/outflow and outflow grid cells are indicated by "X."



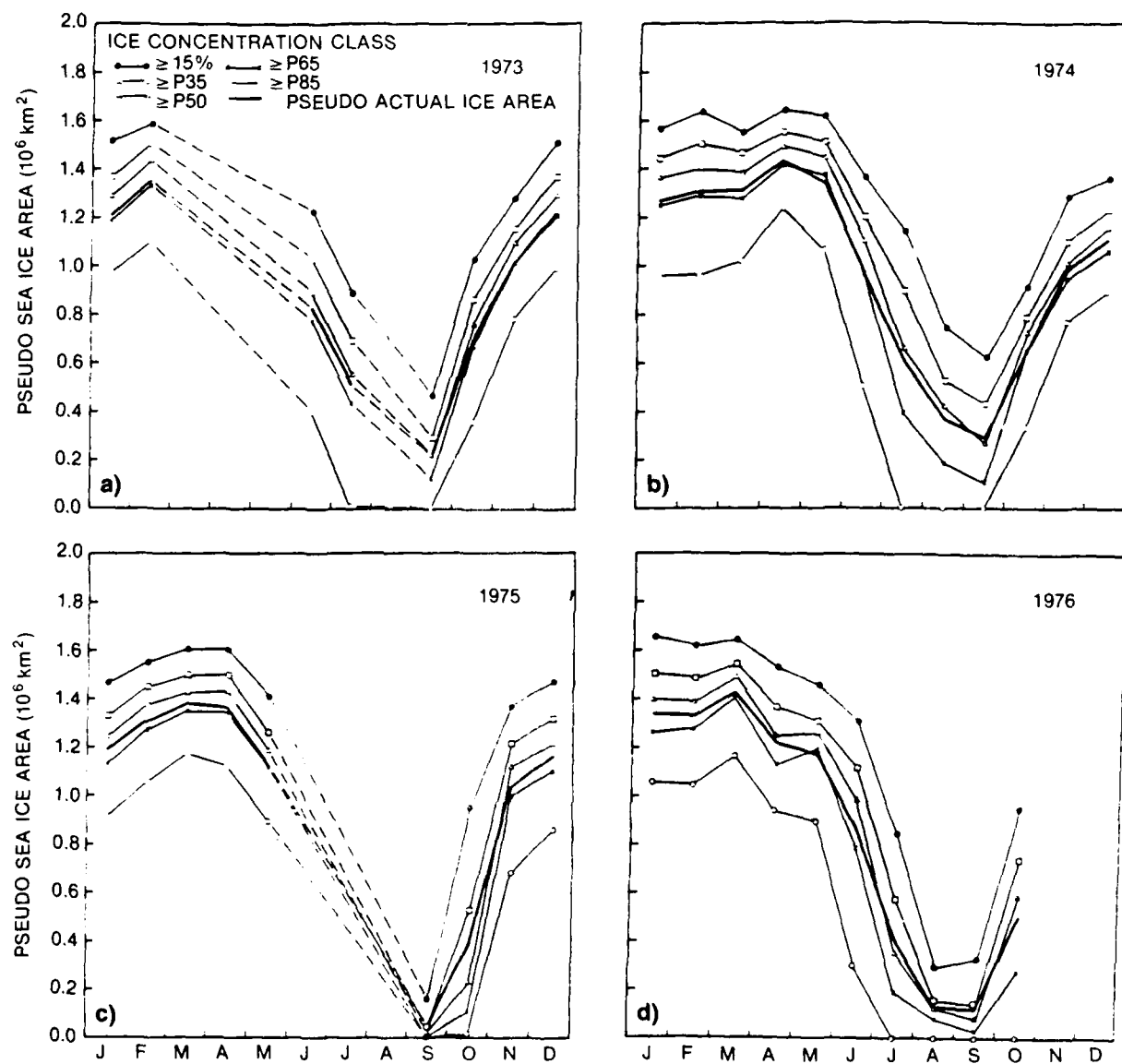
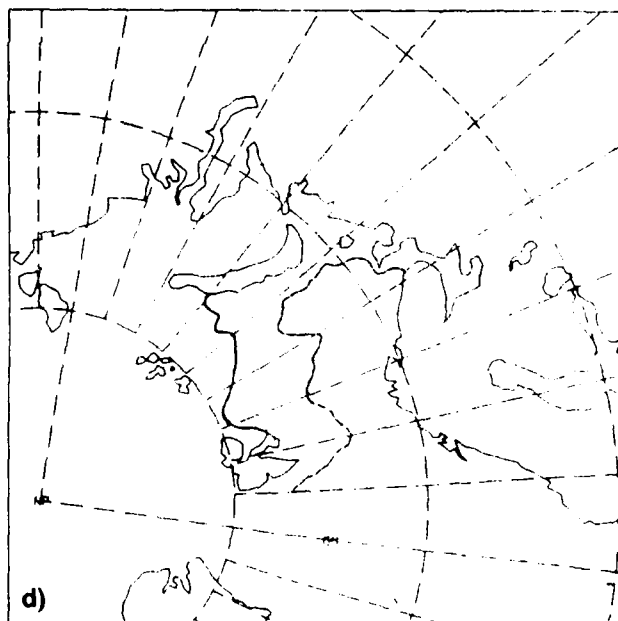
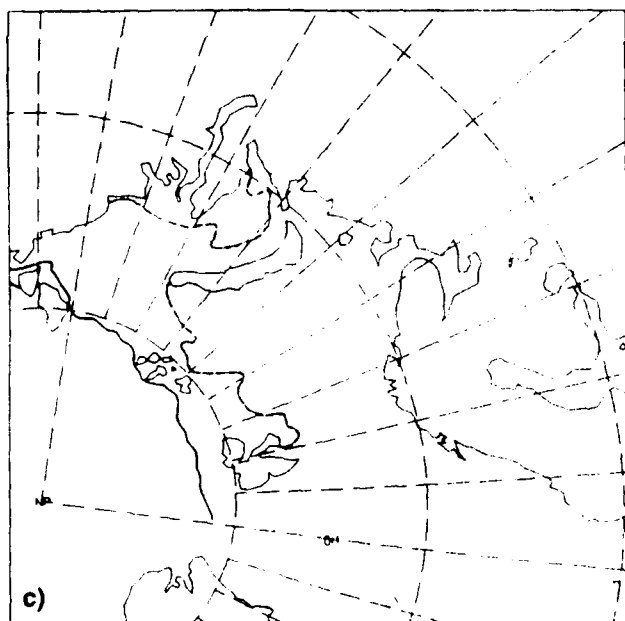
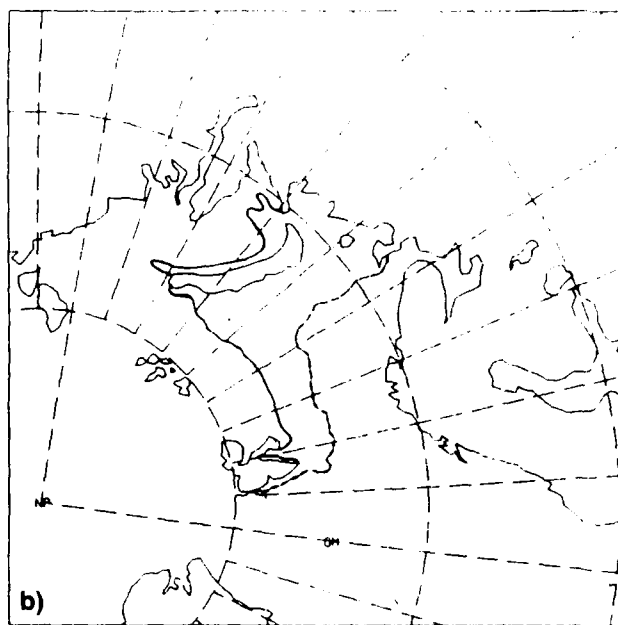
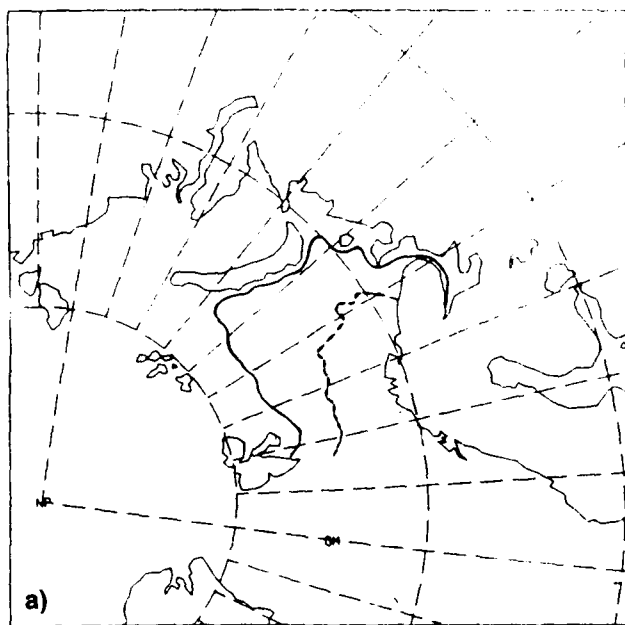


Figure 2. Yearly cycle for the Barents Sea area covered by sea ice for 1973-1976 (from Parkinson et al., 1987). The curves are the ocean area covered with ice greater than 15% (15%), 35% (P35), 50% (P50), 65% (P65), 85% (P85). The pseudo-actual ice area is the integrated ocean surface area covered by sea ice, excluding leads and polynyas.



*Figure 3. Climatological maximum and minimum ice-edge locations from the Navy/NOAA Joint Ice Center for the months of (a) March, (b) June, (c) September and (d) December. The dashed line is the maximum and the solid line the minimum.*

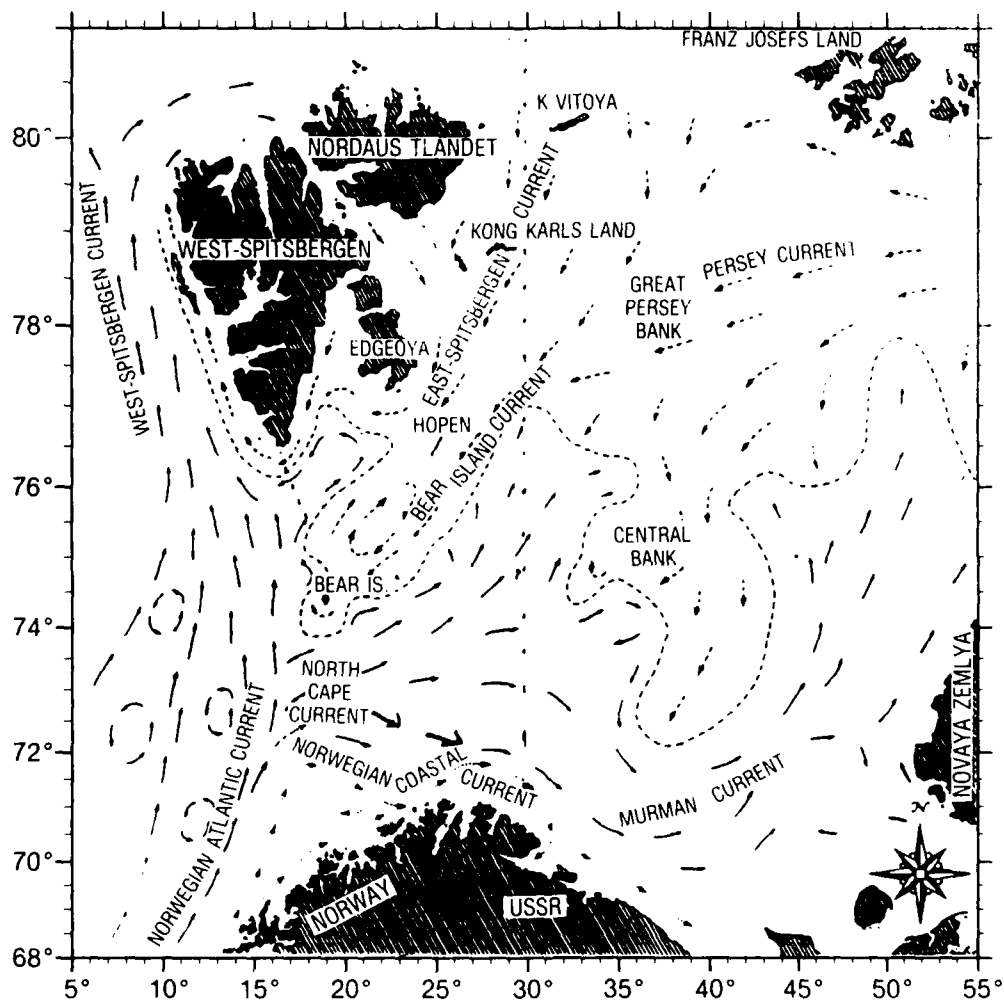


Figure 4. Surface currents system for the Barents Sea from Midttun and Loeng (1987). Solid arrows are Atlantic currents, dashed arrows are Arctic currents, and dotted arrows are coastal currents.

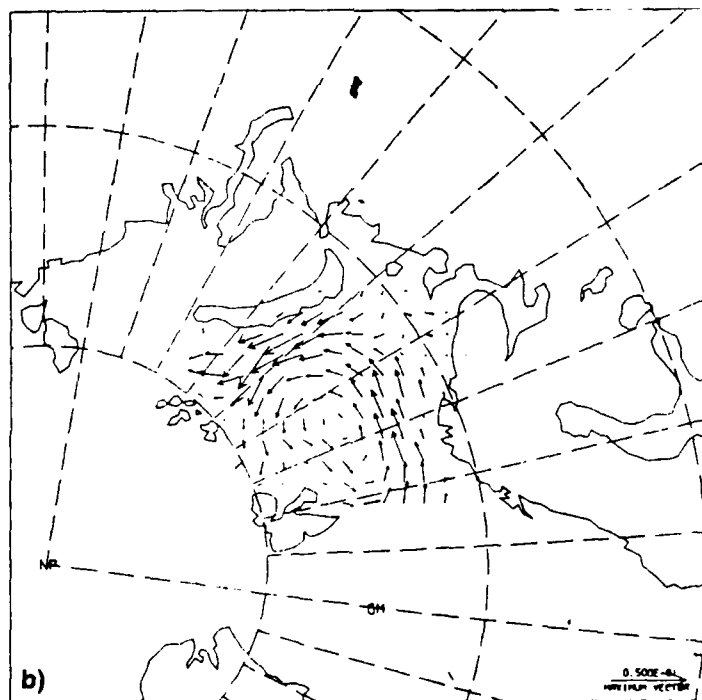
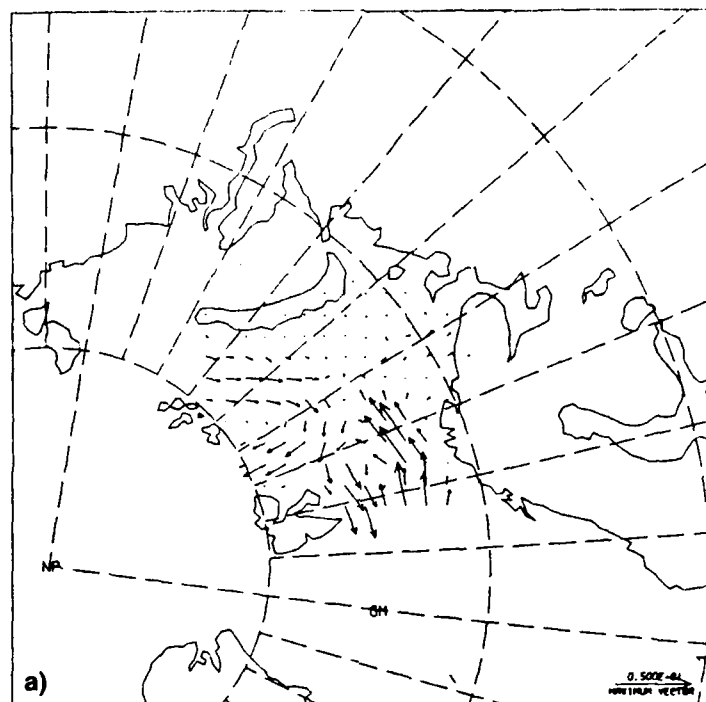


Figure 5. Monthly mean ocean current forcing for the Barents Sea model derived from the Hibler and Bryan (1987) ice-ocean model. Monthly means for (a) February and (b) November are shown. Maximum vector is 5 cm/sec. Every fourth vector is plotted.

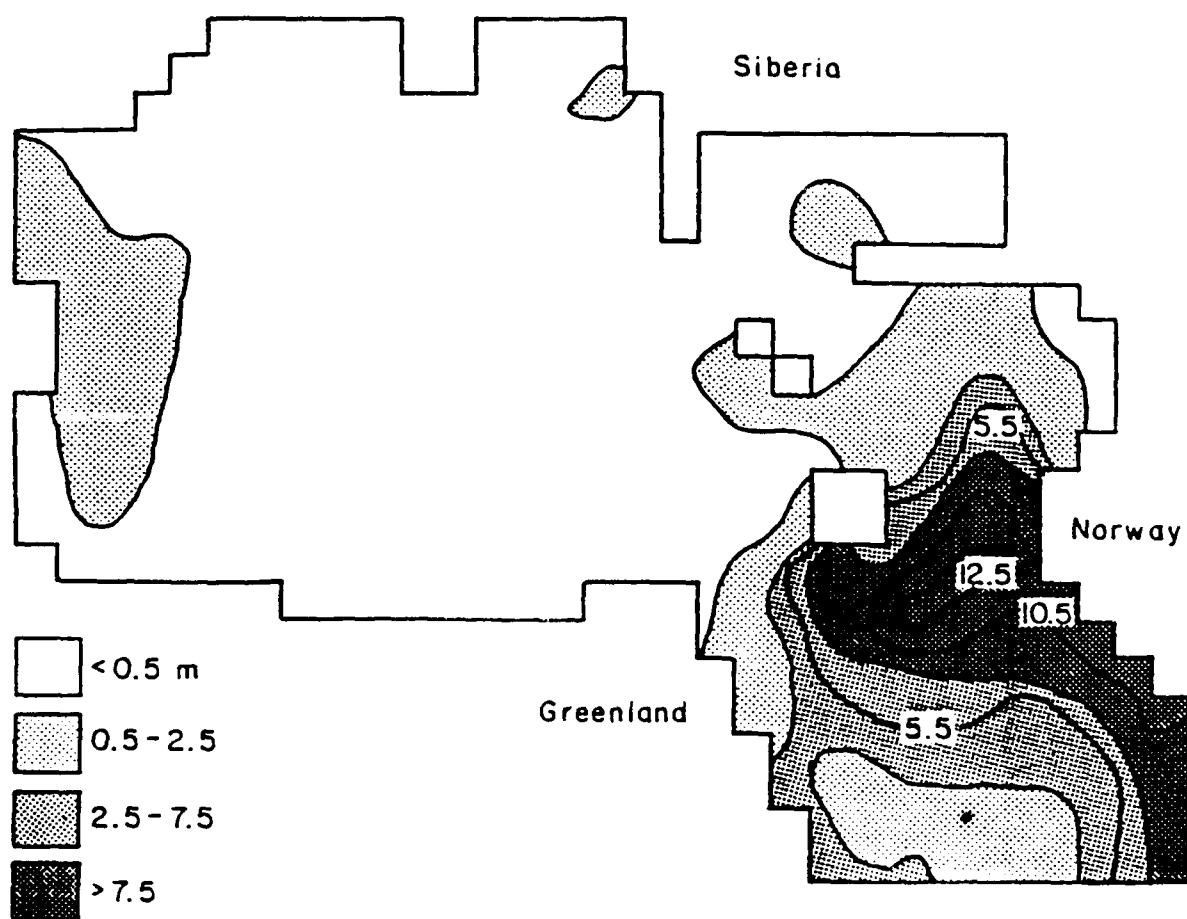


Figure 6. Average annual heat gained by the upper layer of the ocean from the deeper ocean and lateral transport. Contours are in capacity of heat-to-melt meters of ice per year ( $1 \text{ m} \cdot \text{year}^{-1} = 9.57 \text{ W} \cdot \text{m}^{-2}$ ) (from Hibler and Bryan, 1987).

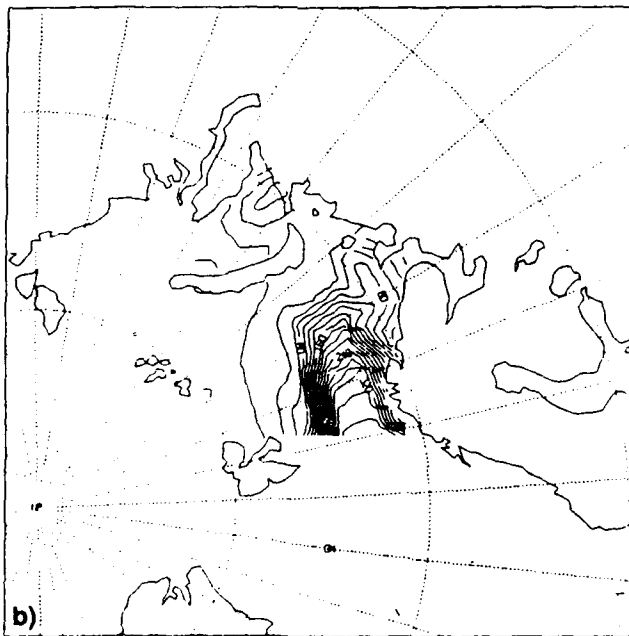
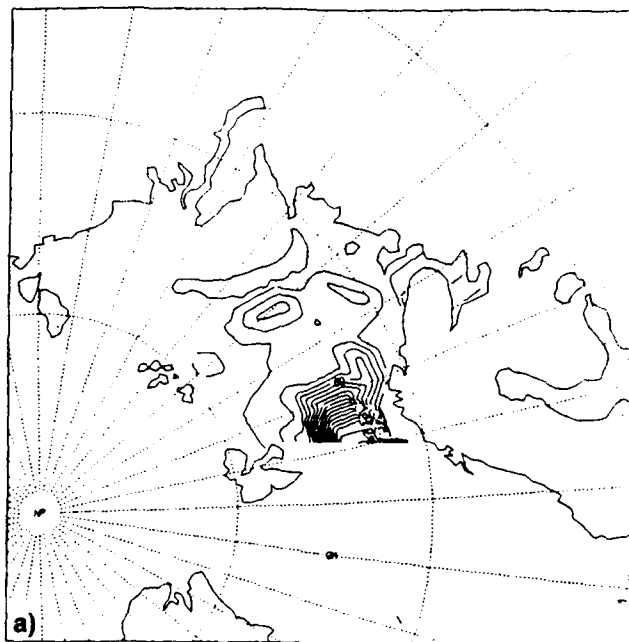


Figure 7. February monthly mean heat fluxes in watts per meter<sup>2</sup> interpolated to the Barents Sea grid from (a) the Hibler and Bryan model and (b) adjusted Hibler and Bryan values.

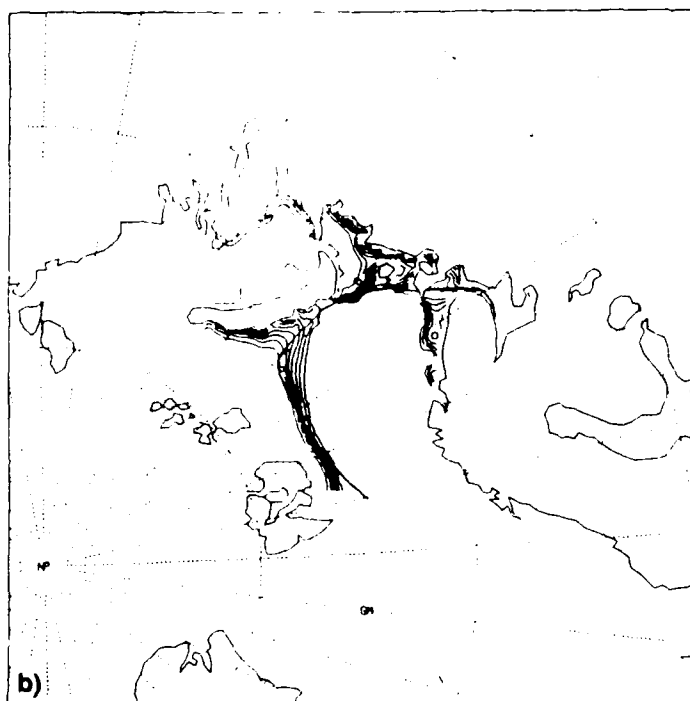
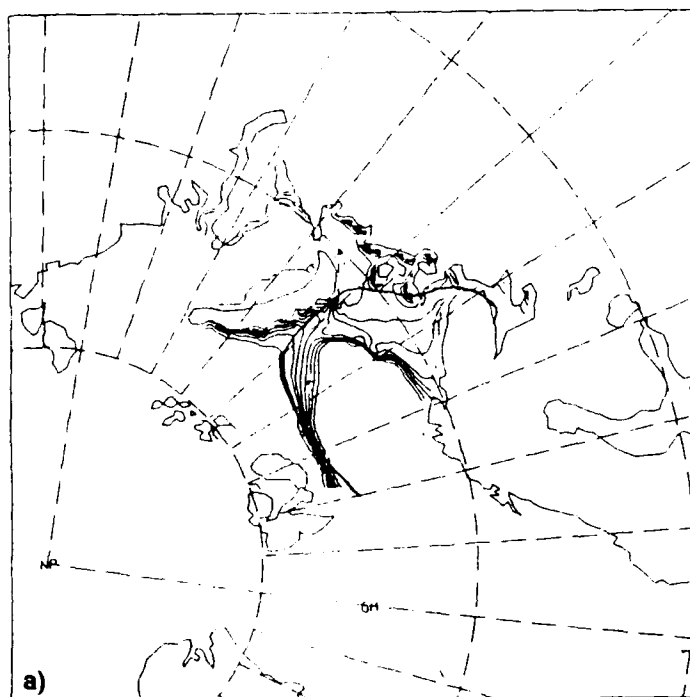


Figure 8. February 1983, monthly mean ice concentration fields for (a) original Hibler and Bryan heat fluxes and (b) the adjusted heat fluxes. The solid black line indicates the mean location of the NPOC ice edge. Contour intervals are in tenths or 10%.

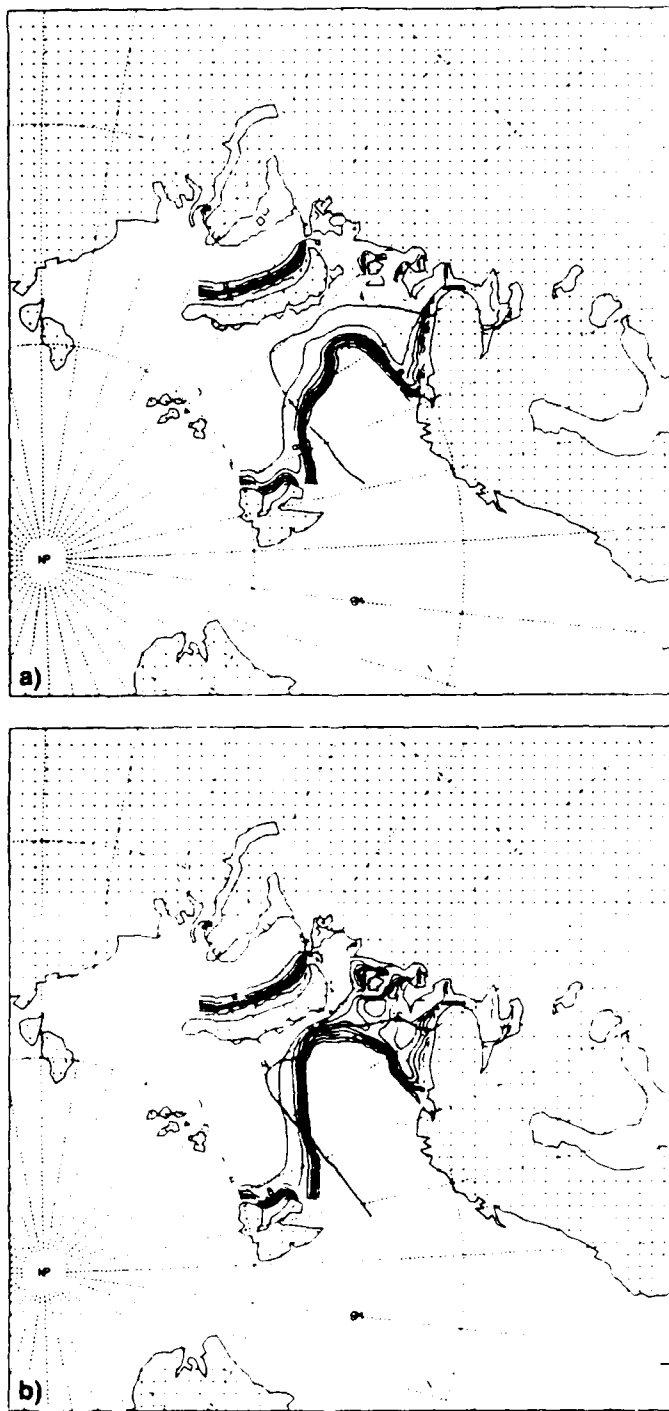


Figure 9. February 1986, monthly mean ice concentration fields for (a) original Hibler and Bryan heat fluxes and (b) the adjusted heat fluxes. The solid black line indicates the mean location of the NPOC ice edge. Contour intervals are in tenths or 10%.



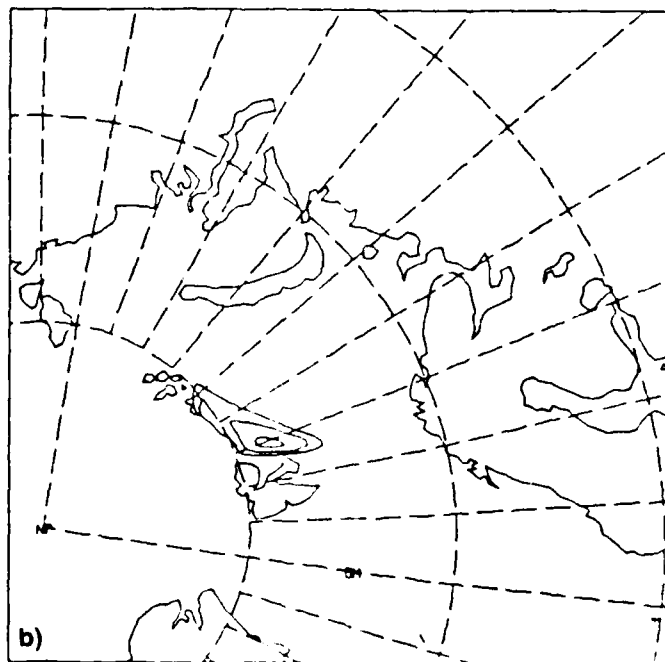
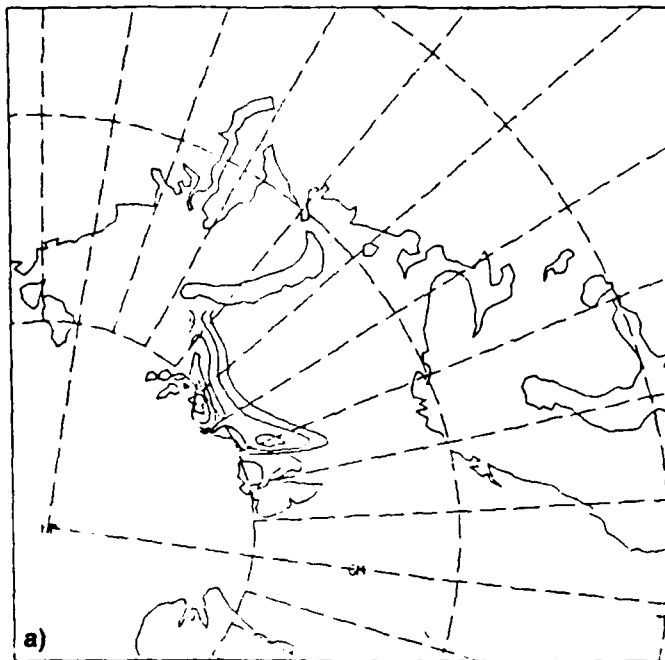


Figure 10. July 1983 ice thickness fields for (a) solid wall boundaries, except for an outflow boundary between Spitzbergen and Norway; and (b) the same case, except that the boundary between Franz Josef Land and Novaya Zemlya is open to inflow and outflow. Contour interval is 0.5 m.

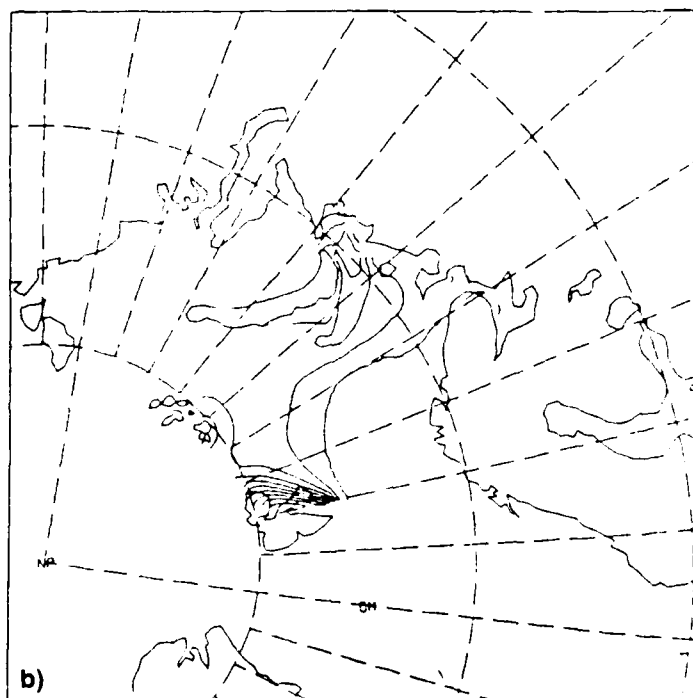
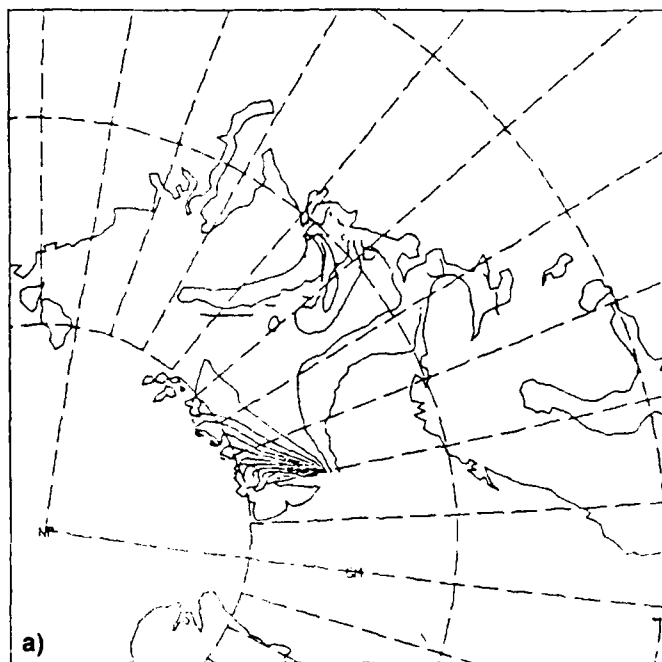


Figure 11. April 1983 ice-thickness fields for (a) the case with boundaries identical to Fig. 10b; and (b) the same case as 10b, but with the boundary between Franz Josef Land and Spitzbergen open to inflow and outflow. Contour interval is 0.5 m.

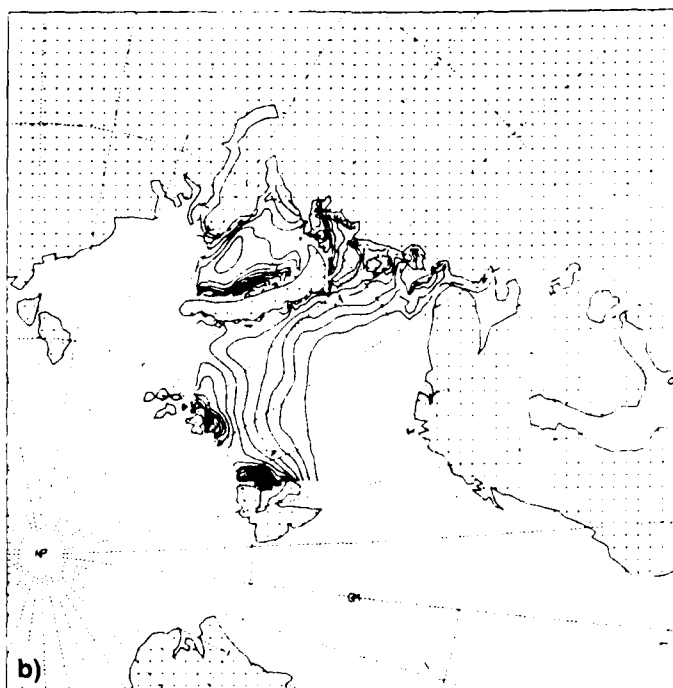
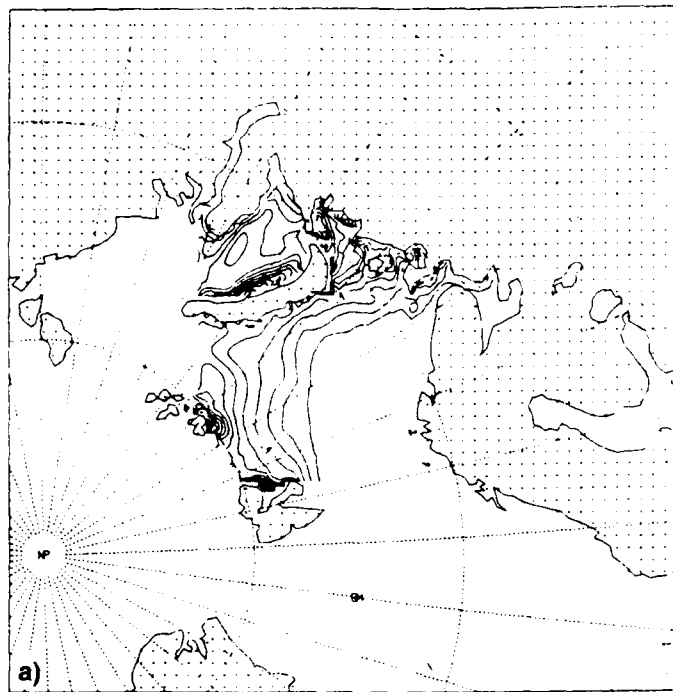


Figure 12. March 1983 monthly mean ice-thickness field from (a) the first spin-up year and (b) the second year. Contour interval is 0.1 m.

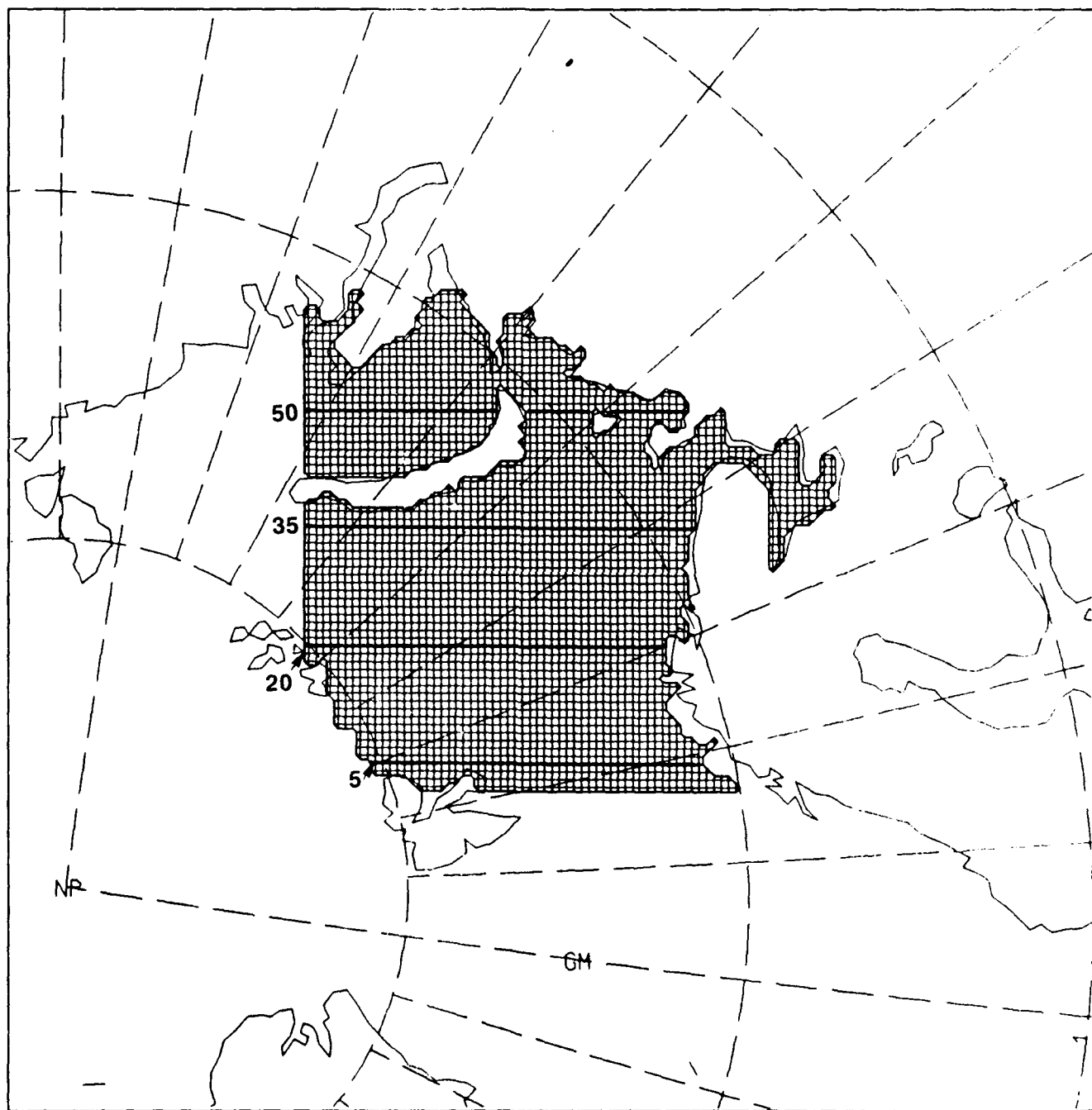


Figure 13. The Barents Sea grid with four transects overlaid at  $J = 5, 20, 35, 50$ .

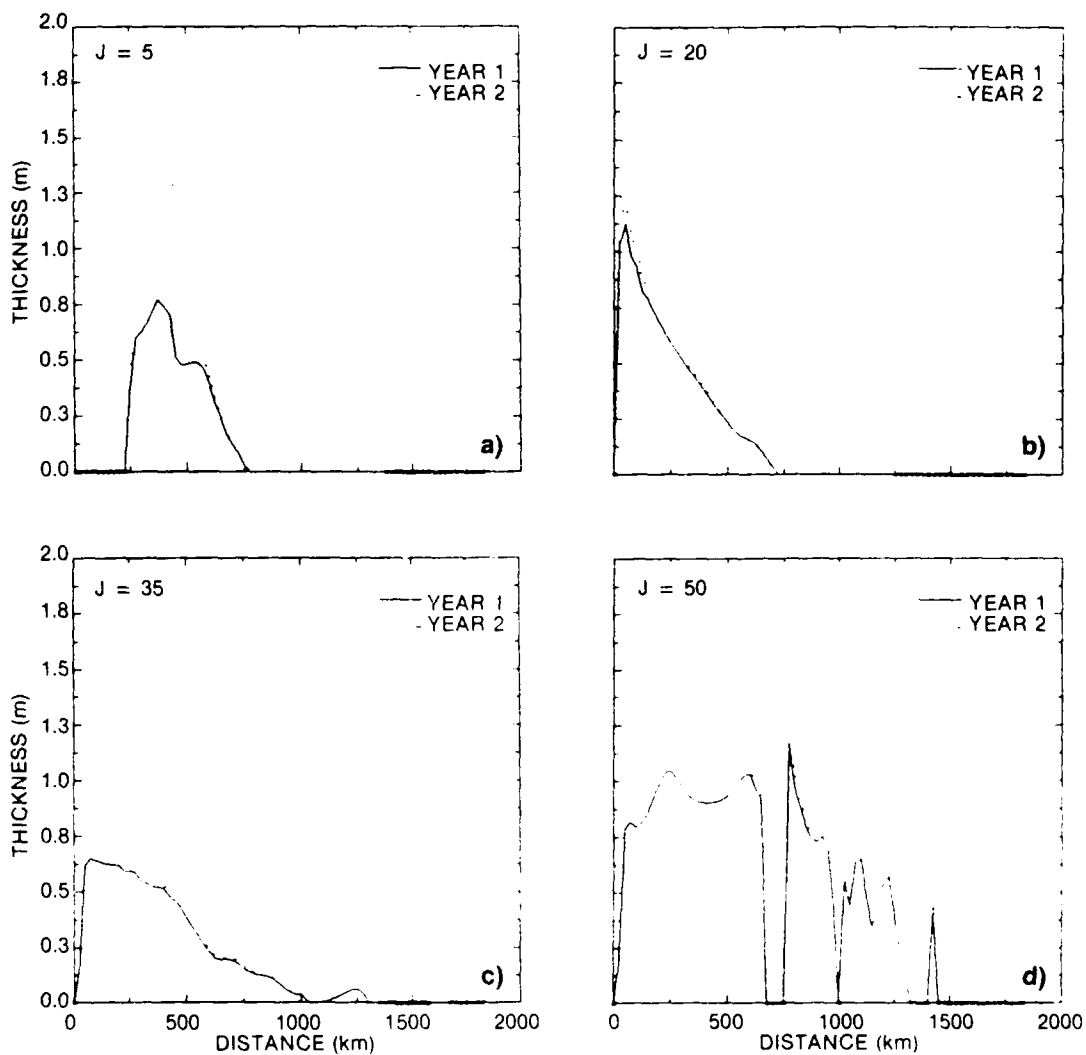


Figure 14. Transects of March monthly mean ice thicknesses at (a)  $J = 5$ , (b)  $J = 20$ , (c)  $J = 35$ , and (d)  $J = 50$ .

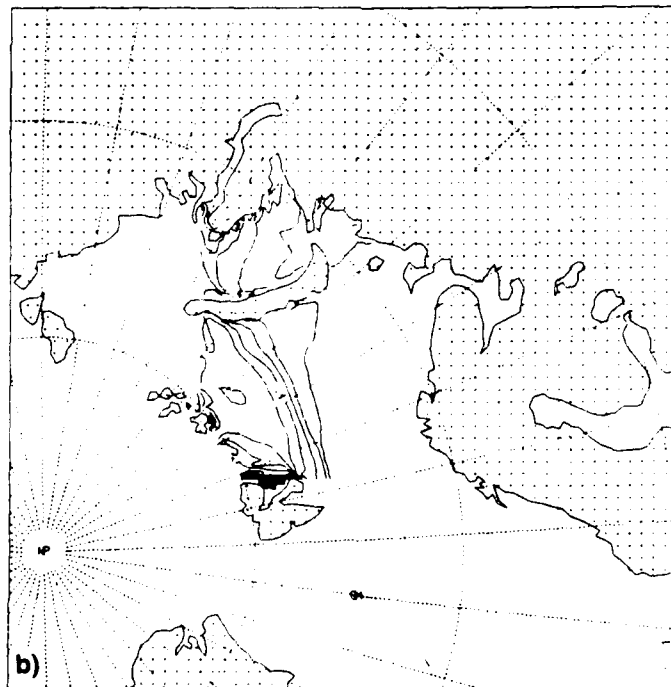
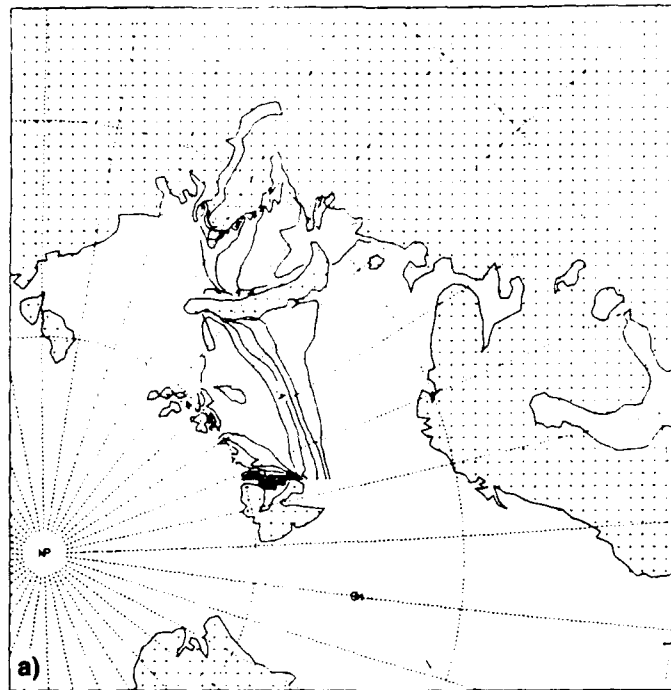


Figure 15. November 1983 monthly mean ice thicknesses from (a) the first year of model spin-up and (b) the second year. Contour interval is 0.1 m.

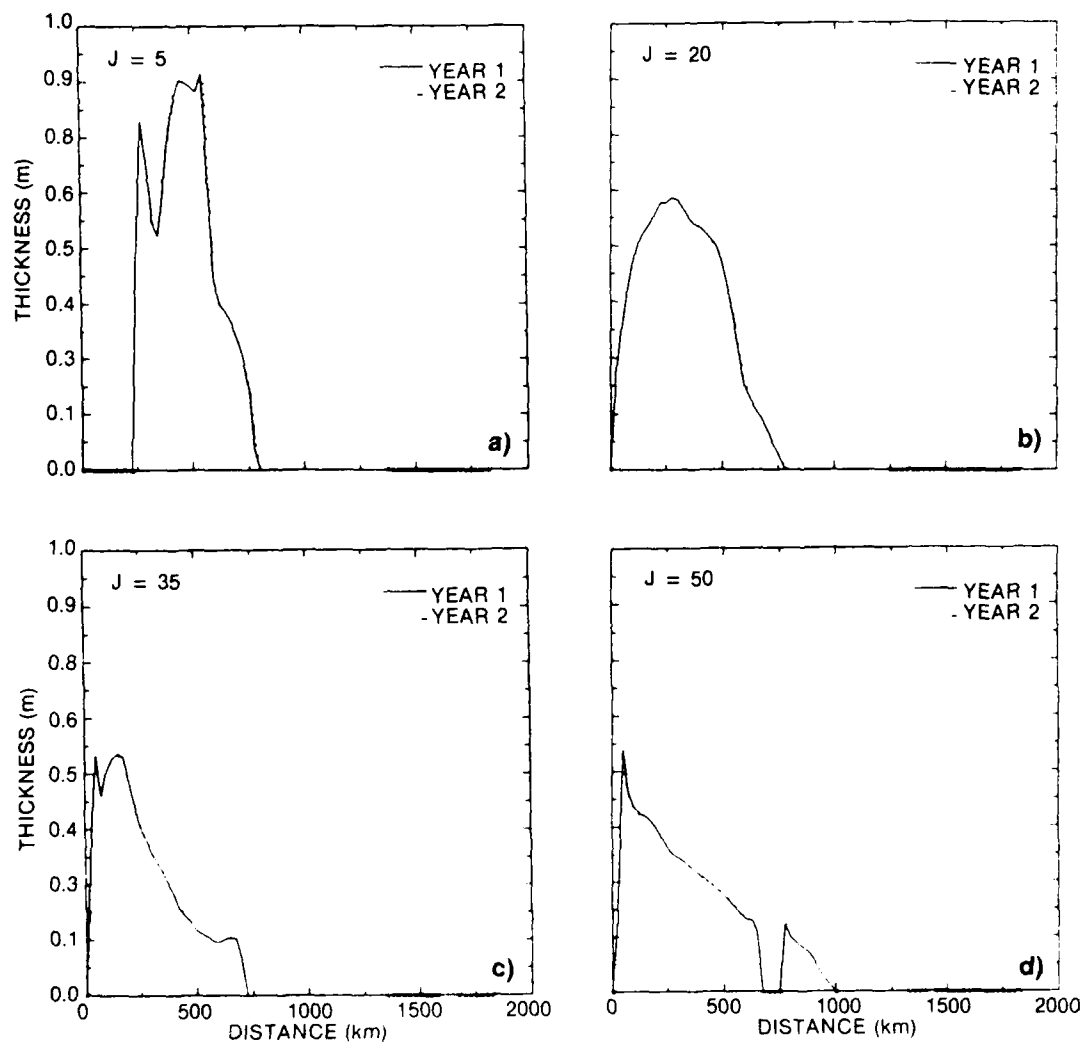


Figure 16. Transects of November monthly mean ice thicknesses at (a)  $J = 5$ , (b)  $J = 20$ , (c)  $J = 35$ , and (d)  $J = 50$ .

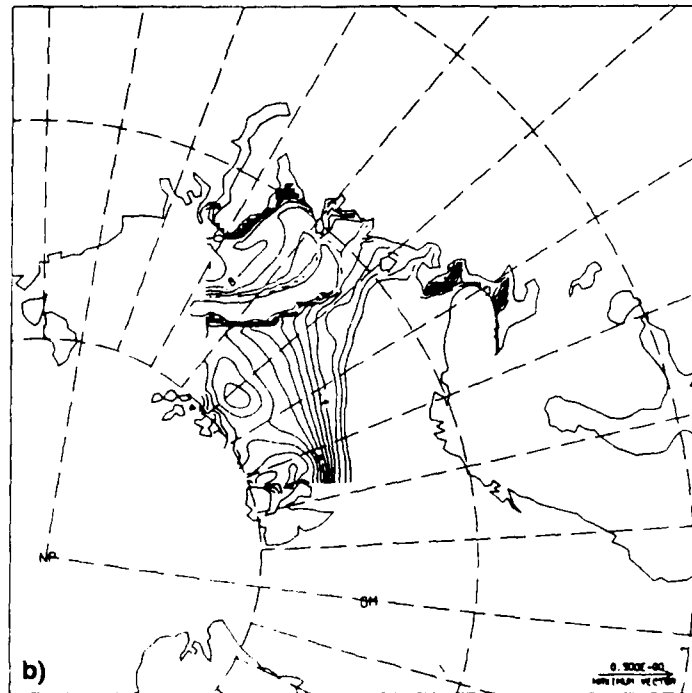
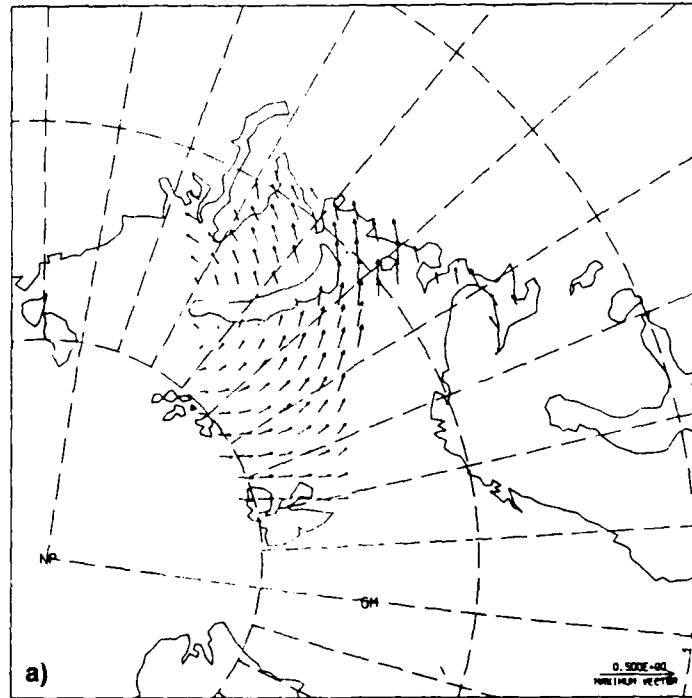


Figure 17. April 1986 monthly mean for (a) ice drift and (b) ice thicknesses. Maximum vector for the ice drift is 50 cm/sec. Every fourth vector is plotted. Contour interval for ice thickness is 0.5 m.



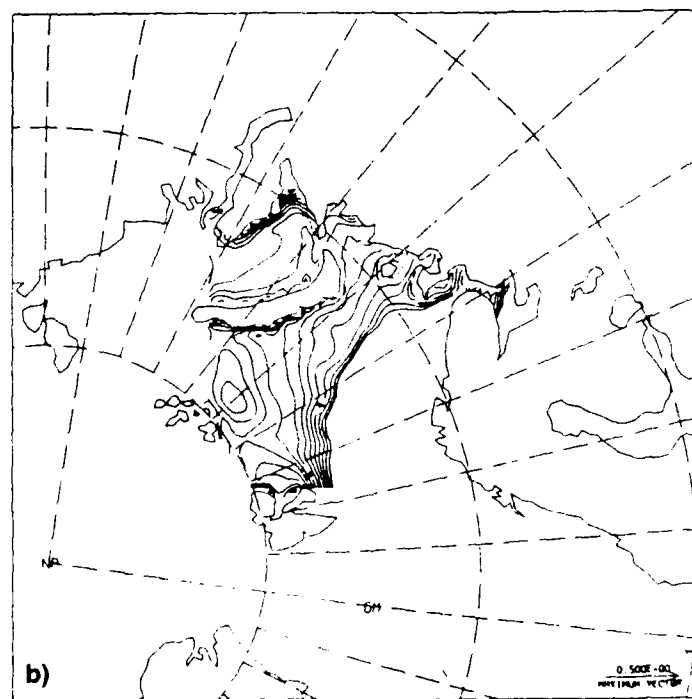
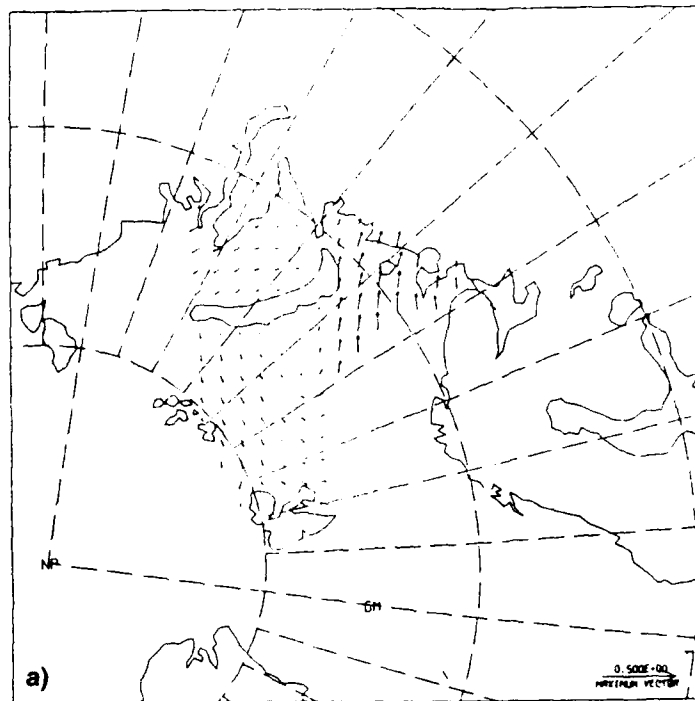


Figure 18. May 1986 monthly mean for (a) ice drift and (b) ice thicknesses. Maximum vector for the ice drift is 50 cm/sec. Every fourth vector is plotted. Contour interval for ice thickness is 0.5 m.

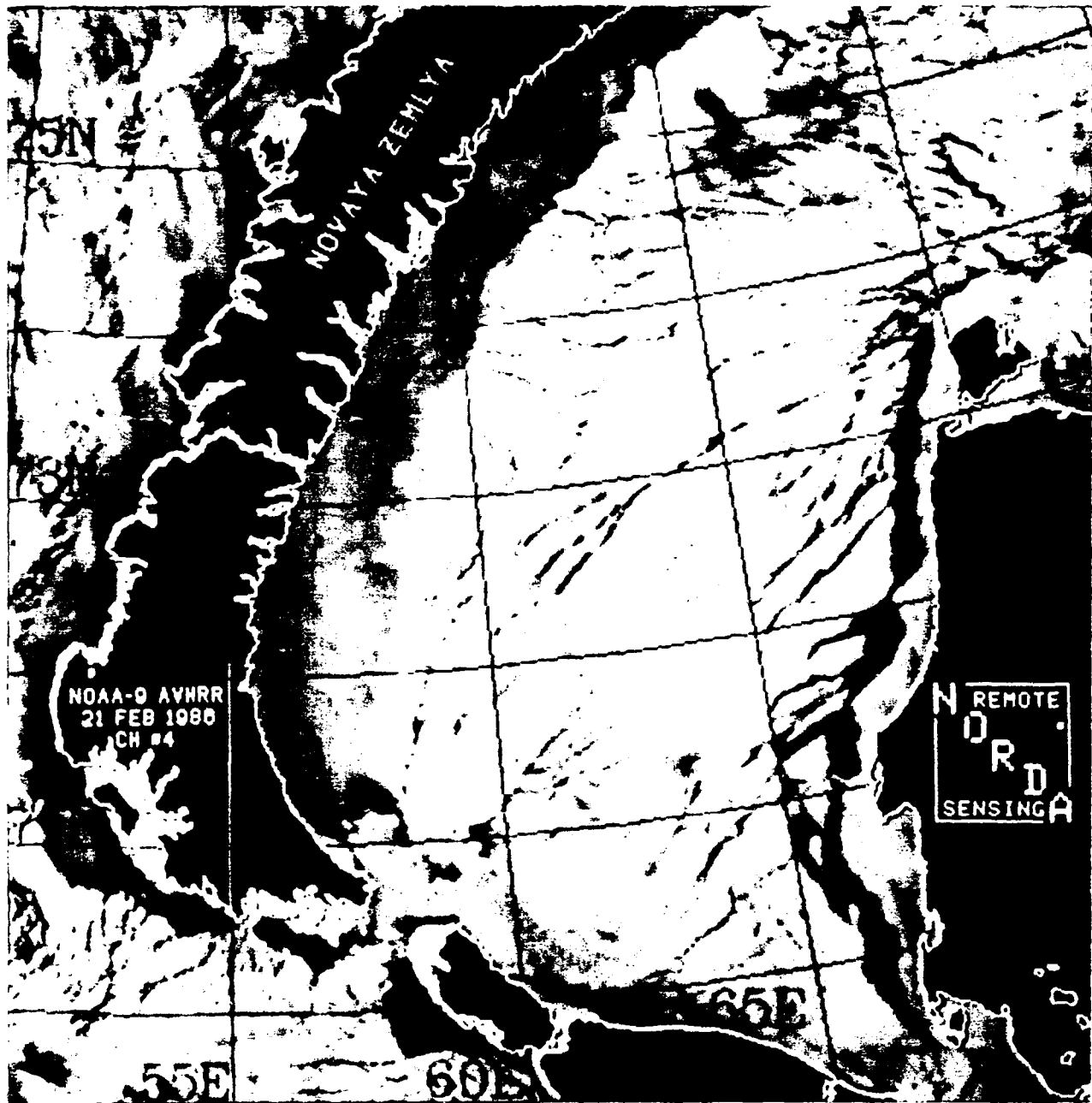


Figure 19. NOAA-9 AVHRR channel 4 imagery for the Kara Sea on 21 February 1986. The eastern side of Novaya Zemlya has new thin ice, indicating that ice was recently pushed away from this coastline (figure courtesy of Jeffrey Hawkins, NORAD).

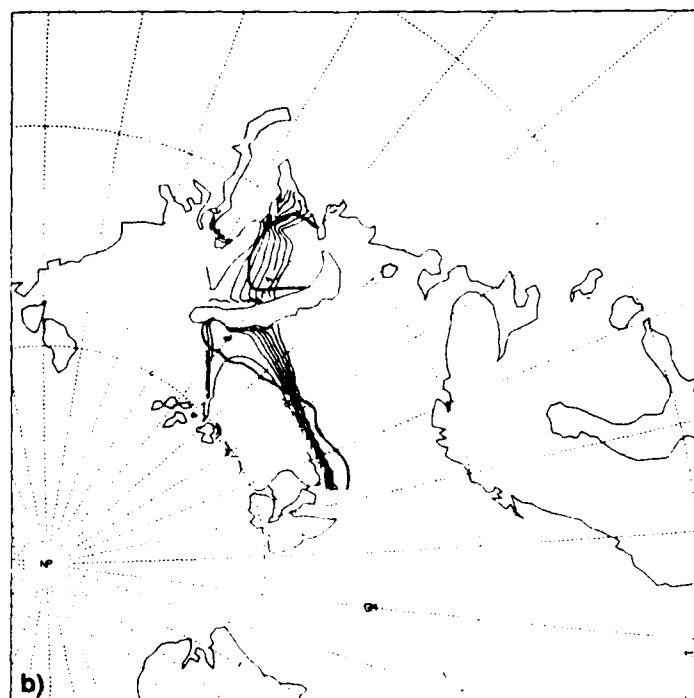
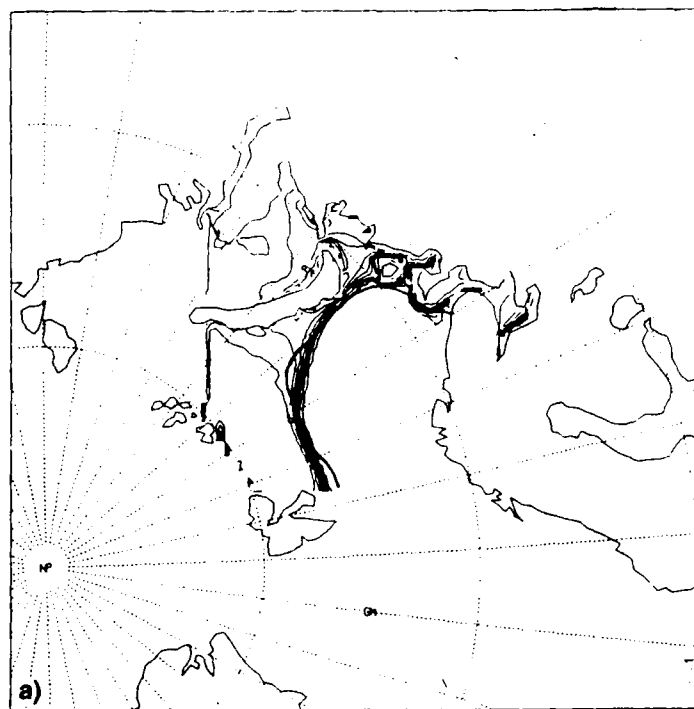


Figure 20. The 1983 ice-concentration fields for (a) March and (b) November. Contour interval is in tenths or 10%. The ice edge from the Navy/NOAA Joint Ice Center is overlaid.

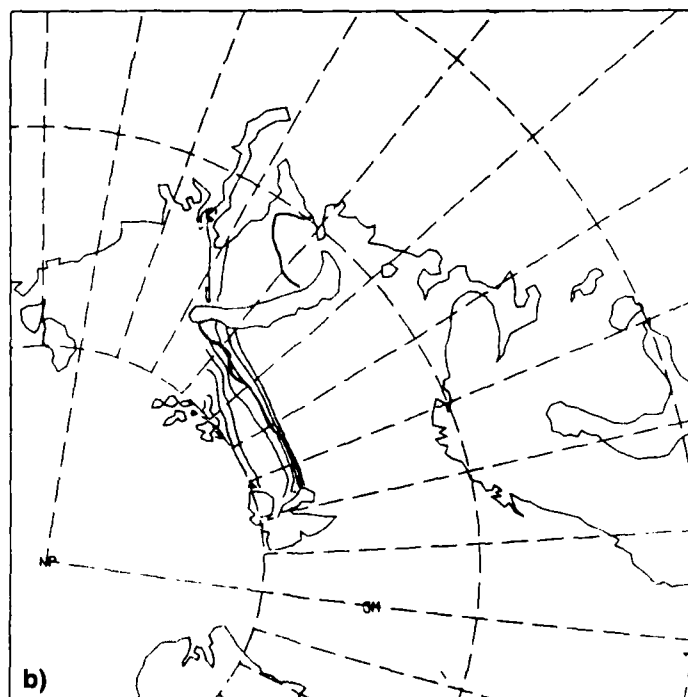
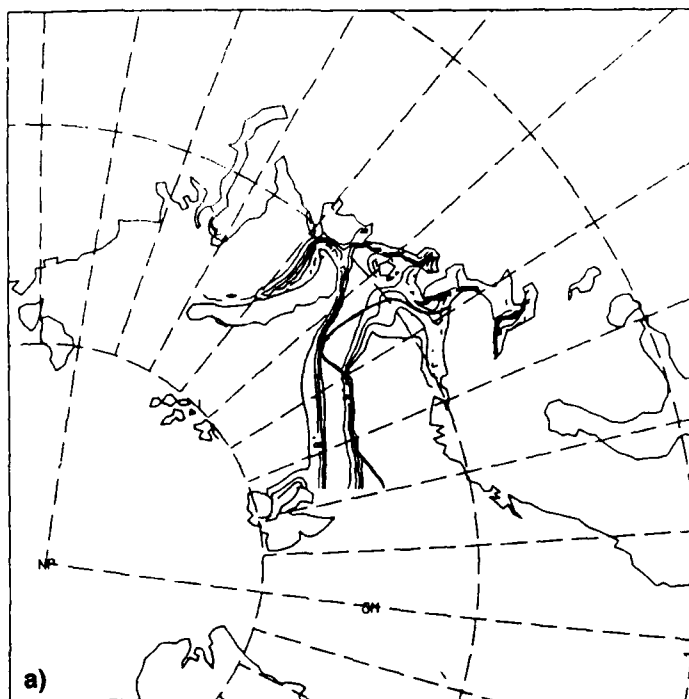


Figure 21. The 1986 ice-concentration fields for (a) March and (b) November. Contour interval is in tenths or 10%. The ice edge from the Navy/NOAA Joint Ice Center is overlaid.

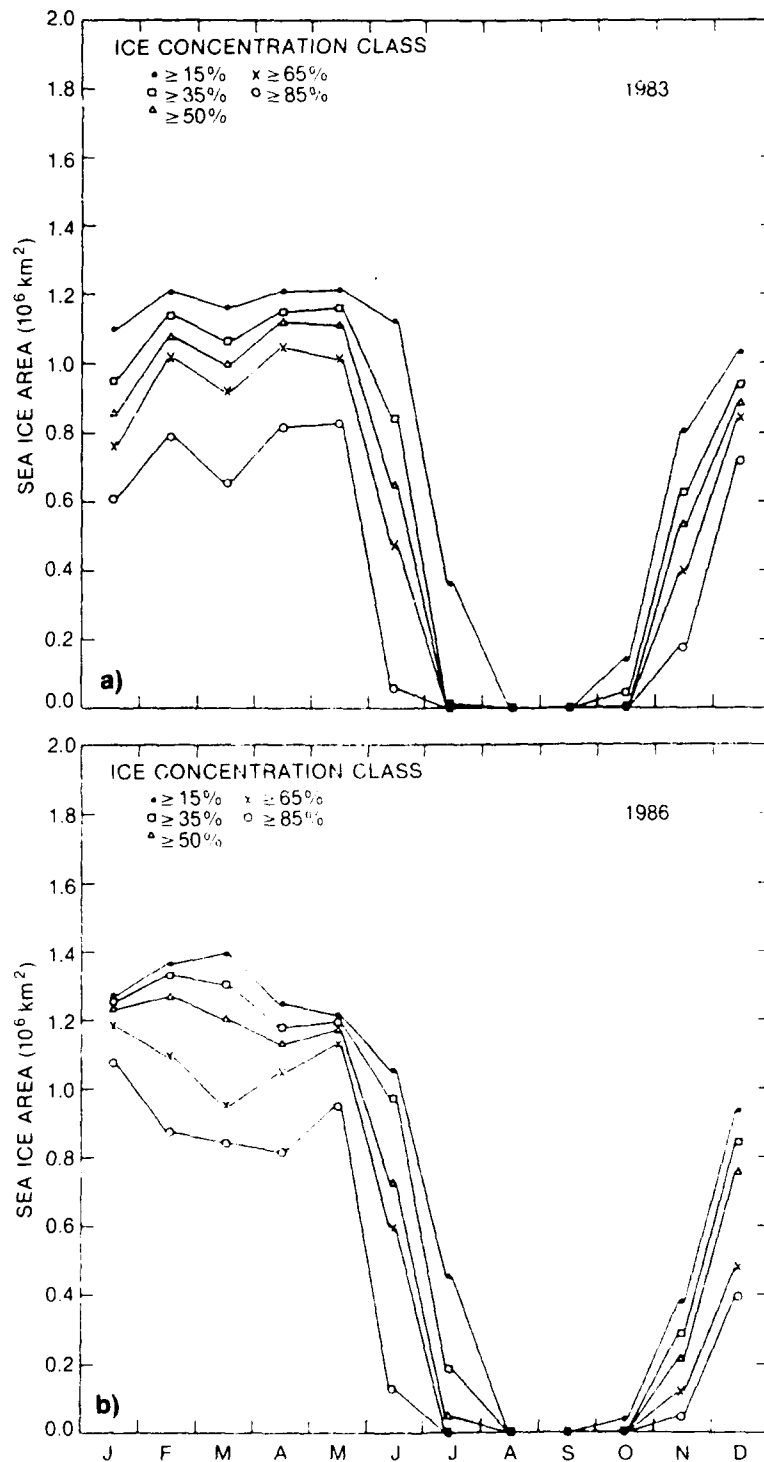


Figure 22. Yearly cycle for the Barents Sea area covered by sea ice for (a) 1983 and (b) 1986 from Barents Sea model 1983 and 1986 results. Curves are the ocean area covered with ice greater than 15%, 35%, 50%, 65%, 85%.

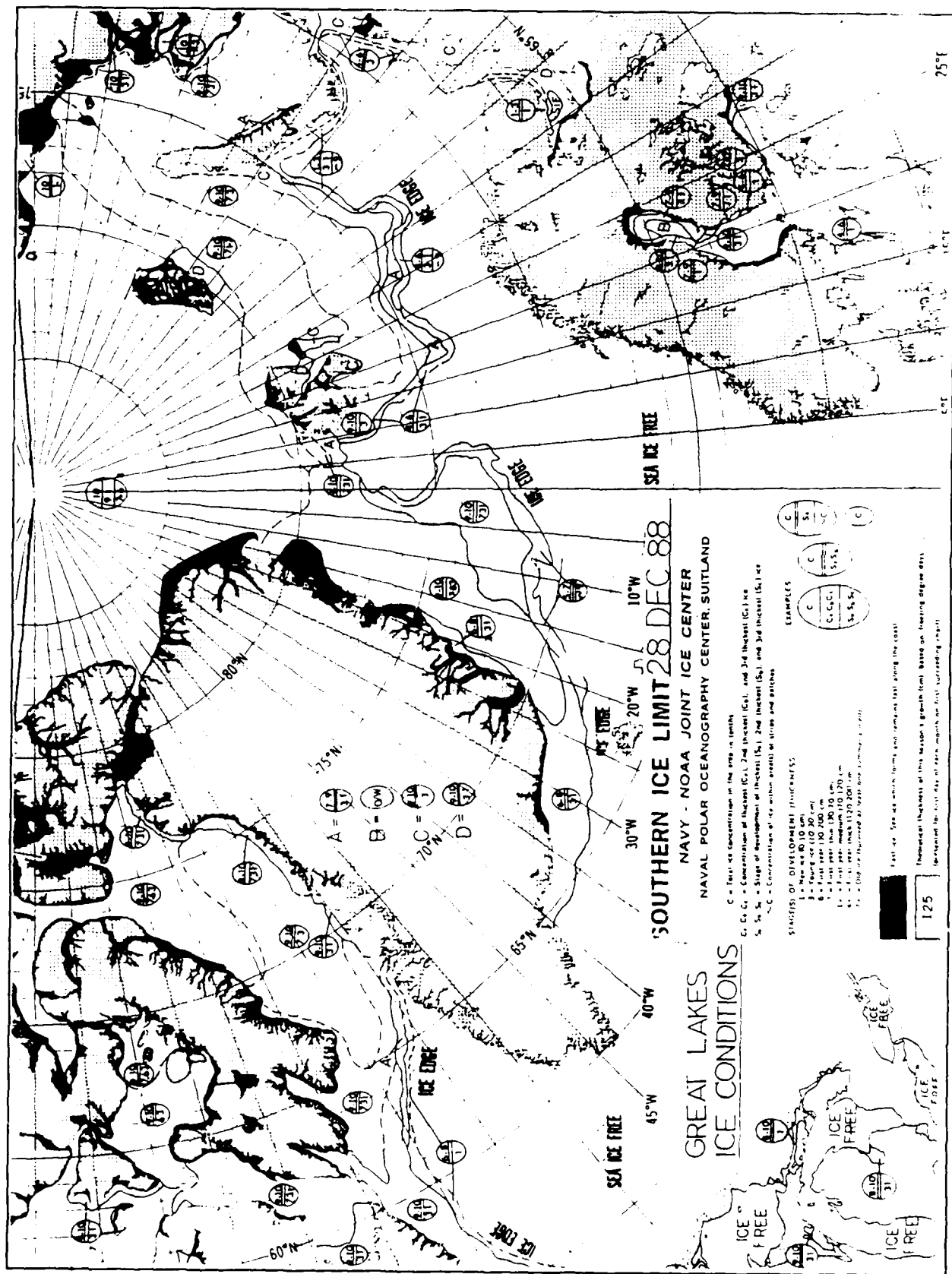


Figure 23. NPOC analysis for the eastern Arctic on 28 December 1988.

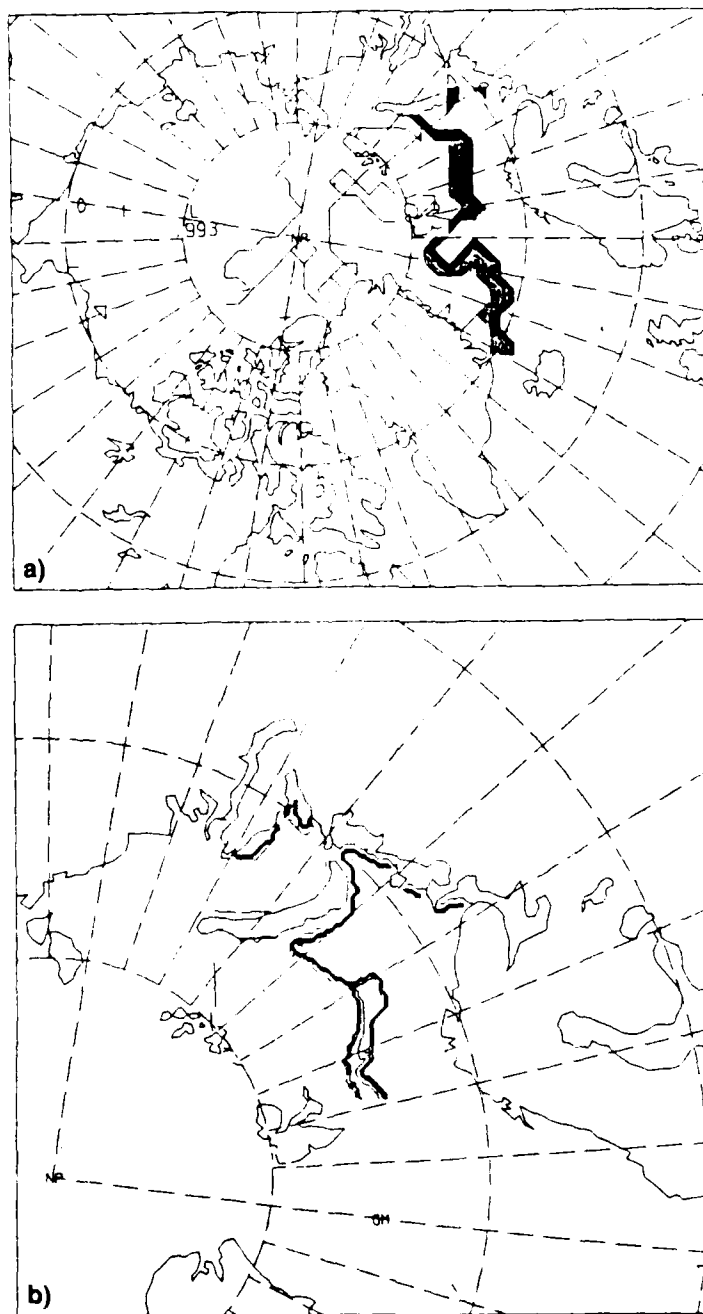


Figure 24. Concentration field from 29 December 1988, immediately after an update from (a) PIPS and (b) RPIPS-B. Contour interval is (a) 5% and (b) 10%.

# Distribution List

Asst Secretary of the Navy  
(Research, Engineering & Systems)  
Navy Department  
Washington DC 20350-1000

Chief of Naval Operations  
Navy Department (OP-02)  
Washington DC 20350-2000

Chief of Naval Operations  
Navy Department (OP-71)  
Washington DC 20350-2000

Director  
National Ocean Data Center  
WSC1 Room 103  
6001 Executive Blvd.  
Attn: G. W. Withee  
Rockville MD 20852

Chief of Naval Operations  
Navy Department (OP-987)  
Washington DC 20350-2000

Oceanographer of the Navy  
Chief of Naval Operations  
Attn: OP-096  
U.S. Naval Observatory  
34th & Mass Ave., NW  
Washington DC 20390-1800

Commander  
Naval Air Development Center  
Warminster PA 18974-5000

Commanding Officer  
Naval Coastal Systems Center  
Panama City FL 32407-5000

Commander  
Space & Naval Warfare Sys Com  
Washington DC 20363-5100

Commanding Officer  
Naval Environmental Prediction  
Research Facility  
Monterey CA 93943-5006

Commander  
Naval Facilities Eng Command  
Naval Facilities Eng Command Headquarters  
200 Stovall St.  
Alexandria VA 22332-2300

Commanding Officer  
Naval Ocean R&D Activity  
Attn: Code 100  
Stennis Space Center MS 39529-5004

Commanding Officer  
Naval Ocean R&D Activity  
Attn: Code 125L (13)  
Stennis Space Center MS 39529-5004

Commanding Officer  
Naval Ocean R&D Activity  
Attn: Code 125P (1)  
Stennis Space Center MS 39529-5004

Commanding Officer  
Naval Ocean R&D Activity  
Attn: Code 105  
Stennis Space Center MS 39529-5004

Commanding Officer  
Naval Ocean R&D Activity  
Attn: Code 115  
Stennis Space Center MS 39529-5004

Commanding Officer  
Naval Ocean R&D Activity  
Attn: Code 200  
Stennis Space Center MS 39529-5004

Commanding Officer  
Naval Ocean R&D Activity,  
Attn: Code 300  
Stennis Space Center MS 39529-5004

Commanding Officer  
Naval Research Laboratory  
Washington DC 20375

Commander  
Naval Oceanography Command  
Stennis Space Center MS 39529-5000

Commanding Officer  
Fleet Numerical Oceanography Center  
Monterey CA 93943-5005

Commanding Officer  
Naval Oceanographic Office  
Stennis Space Center MS 39522-5001

Commander  
Naval Ocean Systems Center  
San Diego CA 92152-5000

Commanding Officer  
ONR Branch Office  
Box 39  
FPO New York NY 09510-0700

Commander  
David W. Taylor Naval Research Center  
Bethesda MD 20084-5000

Commander  
Naval Surface Weapons Center  
Dahlgren VA 22448-5000

Commanding Officer  
Naval Underwater Systems Center  
Newport RI 02841-5047

Superintendent  
Naval Postgraduate School  
Monterey CA 93943

Director of Navy Laboratories  
Rm 1062, Crystal Plaza Bldg 5  
Department of the Navy  
Washington DC 20360

Officer in Charge  
New London Laboratory  
Naval Underwater Sys Cen Det  
New London CT 06320

Director  
Office of Naval Research  
Attn: Code 10  
800 N. Quincy St.  
Arlington VA 22217-5000

Director  
Woods Hole Oceanographic Inst  
P.O. Box 32  
Woods Hole MA 02543

University of California  
Scripps Institute of Oceanography  
P.O. Box 6049  
San Diego CA 92106

Officer in Charge  
Naval Surface Weapons Center Det  
White Oak Laboratory  
10901 New Hampshire Ave  
Attn: Library  
Silver Spring MD 20903-5000

Commanding Officer  
Fleet Anti-Sub Warfare Training Center, Atlantic  
Naval Station  
Norfolk VA 23511-6495



Brooke Farquhar  
NORDA Liaison Office  
Crystal Plaza #5, Room 802  
2211 Jefferson Davis Hwy.  
Arlington VA 22202-5000

Director  
Defense Mapping Agency Sys Cen  
Attn: SGWN  
12100 Sunset Hill Rd. #200  
Reston VA 22090-3207

NORDA  
Code 125 EX  
Stennis Space Center MS 39529-5004  
(Unlimited only)

Director  
Office of Naval Technology  
Attn: Dr. P. Selwyn, Code 20  
800 N. Quincy St.  
Arlington VA 22217-5000

Director  
Office of Naval Technology  
Attn: Dr. C. V. Votaw, Code 234  
800 N. Quincy St.  
Arlington VA 22217-5000

Director  
Office of Naval Technology  
Attn: Dr. M. Briscoe, Code 229  
800 N. Quincy St.  
Arlington VA 22217-5000

Director  
Office of Naval Research  
Attn: Dr. E. Hartwig, Code 112  
800 N. Quincy St.  
Arlington VA 22217-5000

Director  
Office of Naval Research  
Attn: Code 12  
800 N. Quincy St.  
Arlington VA 22217-5000

Director  
Office of Naval Research  
Attn: Dr. E. Silva, Code 10D/10P  
800 N. Quincy St.  
Arlington VA 22217-5000

Chief of Naval Operations  
Navy Department (OP-0962X)  
Attn: Mr. R. Feden  
Washington DC 20350-2000

Commander  
Naval Sea Systems Command  
Naval Sea Systems Command Headquarters  
Washington DC 20362-5101

Commanding Officer  
Naval Civil Engineering Laboratory  
Port Hueneme CA 93043

Commander  
Naval Air Systems Command  
Naval Air Systems Command Headquarters  
Washington DC 20361-0001

Pennsylvania State University  
Applied Research Laboratory  
P.O. Box 30  
State College PA 16801

University of Texas at Austin  
Applied Research Laboratories  
P.O. Box 8029  
Austin TX 78713-8029

Johns Hopkins University  
Applied Physics Laboratory  
Johns Hopkins Rd.  
Laurel MD 20707

University of Washington  
Applied Physics Laboratory  
1013 Northeast 40th St.  
Seattle WA 98105

UNCLASSIFIED

SECURITY CLASSIFICATION OF THIS PAGE

REPORT DOCUMENTATION PAGE				
1a REPORT SECURITY CLASSIFICATION <b>Unclassified</b>		1d RESTRICTIVE MARKINGS <b>None</b>		
2a SECURITY CLASSIFICATION AUTHORITY		3 DISTRIBUTION/AVAILABILITY OF REPORT Approved for public release, distribution is unlimited. Naval Ocean Research and Development Activity Stennis Space Center Mississippi 39529-5994.		
2b DECLASSIFICATION/DOWNGRADING SCHEDULE				
4 PERFORMING ORGANIZATION REPORT NUMBER(S) <b>NORDA Report 182</b>		5 MONITORING ORGANIZATION REPORT NUMBER(S) <b>NORDA Report 182</b>		
6 NAME OF PERFORMING ORGANIZATION <b>Naval Ocean Research and Development Activity</b>		7a NAME OF MONITORING ORGANIZATION <b>Naval Ocean Research and Development Activity</b>		
6c ADDRESS (City, State, and ZIP Code) <b>Ocean Science Directorate Stennis Space Center, Mississippi 39529-5004</b>		7b ADDRESS (City, State, and ZIP Code) <b>Ocean Science Directorate Stennis Space Center, Mississippi 39529-5004</b>		
8a NAME OF FUNDING/SPONSORING ORGANIZATION <b>Commander—Space and Naval Warfare Systems Command</b>	8b OFFICE SYMBOL (If applicable)	9 PROCUREMENT INSTRUMENT IDENTIFICATION NUMBER		
8c ADDRESS (City, State, and ZIP Code) <b>Code PDW 106-8 Washington, D.C. 20361</b>		10 SOURCE OF FUNDING NOS		
		PROGRAM ELEMENT NO <b>63207N</b>	PROJECT NO <b>00513</b>	TASK NO <b>999</b>  WORK UNIT NO <b>DN894428</b>
11 TITLE (Include Security Classification) <b>The Regional Polar Ice Prediction System—Barents Sea (RPIPS-B): A Technical Description</b>				
12 PERSONAL AUTHOR(S) <b>Ruth H. Preller, Shelley Riedlinger, and *Pamela G. Posey</b>				
13a TYPE OF REPORT <b>Final</b>	13b TIME COVERED From To	14 DATE OF REPORT (Yr. Mo. Day) <b>May 1989</b>	15 PAGE COUNT <b>38</b>	
16 SUPPLEMENTARY NOTATION <b>*Berkeley Research Associates, P.O. Box 852, Springfield, Virginia 22150</b>				
17 SUBJECT TERMS (Continue on reverse if necessary and identify by block number)				
		<b>sea ice forecasting, sea ice models, Barents Sea, sea ice analysis</b>		
18 ABSTRACT (Continue on reverse if necessary and identify by block number) The hydrodynamic/thermodynamic Arctic sea-ice model designed by W. D. Hibler of the Cold Regions Research and Engineering Laboratory (CRREL) has been adapted to the Barents Sea. This model is driven by atmospheric forcing from the Naval Operational Global Atmospheric Prediction System (NOGAPS) and oceanic forcing from the Hibler and Bryan coupled ice-ocean model. This high-resolution model (25 km), which covers the entire Barents Sea and the western half of the Kara Sea, uses a 6-hour time step. Development of this model required the design of new ice inflow/outflow boundary conditions, which use the ice thickness fields from the Polar Ice Prediction System (PIPS) when inflow is indicated. Model results show good agreement with such data as the Naval Polar Oceanography Center's (NPOC) analysis of ice concentration and concentrations derived from passive microwave data. The model has a tendency, however, to melt ice too quickly in summer and to grow it back too slowly in the fall. Planned improvements in the atmospheric and oceanic forcing should correct this problem. The high resolution of the Barents Sea model enables it to predict the ice edge, ice growth and decay, and the movement of ice near land boundaries with greater accuracy than does the PIPS model. The Regional Polar Ice Prediction System for the Barents Sea (RPIPS-B) is the forecast system designed to run at the Fleet Numerical Oceanography Center (FNOC) based on the Barents Sea ice model. RPIPS-B is updated weekly by the NPOC analysis of ice concentration. The forecast system, presently in its "operational checkout" phase, is being made ready for a winter-spring operational test.				
20 DISTRIBUTION/AVAILABILITY OF ABSTRACT UNCLASSIFIED/UNLIMITED SAME AS RPT <input checked="" type="checkbox"/> DTIC USERS		21 ABSTRACT SECURITY CLASSIFICATION <b>Unclassified</b>		
22a NAME OF RESPONSIBLE INDIVIDUAL <b>R. H. Preller</b>		22b TELEPHONE NUMBER (Include Area Code) <b>(601) 688-5444</b>	22c OFFICE SYMBOL <b>Code 322</b>	